Voltage-controlled instability transitions and competitions in a finitely deformed dielectric elastomer tube

Yipin Su [a,b]

[a] *Department of Engineering Mechanics, Zhejiang University, Hangzhou 310027, PR China*
[b] *School of Mathematics, Statistics and Applied Mathematics, NUI Galway, University Road, Galway, Ireland*

ARTICLE INFO

ABSTRACT

This work compares the transition and competitive mechanism between three types of instabilities of an incompressible dielectric tube: wrinkling, pull-in instability and electric breakdown. We also see how to select one type of instability mode on demand. First, we investigate the finite response and the wrinkling of a tube subject to a combination of applied radial voltage, torsion and axial force (or stretch). We use the surface impedance matrix method to determine the wrinkling threshold, and obtain the corresponding two-dimensional pattern shape of wrinkled surface. Second, we look at illustrative numerical calculations for ideal Mooney-Rivlin dielectrics and study the effects of actuation methods, electric voltage, torsion and geometrical parameters on the three types of instabilities. Results show that the deformation of the solid will influence the true electric field in the solid, and induce competitive effects between the applied voltage and the mechanical loading. We find that in addition to the expected contractile buckling, buckling may also occur in extension in an electrically actuated dielectric tube, a departure from the purely elastic wrinkling. Moreover, the electro-elastic behavior of the DE elastomer can be enhanced by introducing torsion. We also find that large stable actuation can be achieved and that the wrinkling pattern can be selected on demand in the tube by finely tuning the actuation, voltage, torsion and geometry, without encountering material failure.

1. Introduction

Dielectric elastomers (DEs) have received extensive attention due to their promising applications in biomedical engineering, soft robots, adaptive optics, high-performance actuators and sensors, etc. (Brochu & Pei, 2012; Duduta, Hajiesmaili, Zhao, Wood, & Clarke, 2019; O'Halloran, O'malley, & McHugh, 2008; Rasmussen, 2012). Pelrine, Kornbluh, and Joseph (1998) first proposed the so-called *tubular DE actuator* consisting of a thin-walled cylindrical elastomeric tube sandwiched between two compliant electrodes on its inner and outer faces. With the application of a voltage through the electrodes, the interposed tube wall is squeezed, causing a radial expansion and an axial elongation (Cameron, Szabo, Johnstone, Massey, & Leidner, 2008; Carpi & De Rossi, 2004). By cyclically activating and de-activating the DE tube, the inner volume of the tube can be changed repeatedly to control the inlet and outlet of gases or liquids. One potential use of such mechanism is for manufacturing large-volume pumps (Brown & Lai, 2009; Wang et al., 2018). Tubular DE actuators can be manufactured through well-established industrial processes, such as extrusion and flexible dip-coating techniques. (Arora, Ghosh, & Muth, 2007; Stoyanov, Kofod, & Gerhard, 2008). Compared with planar DE actuators, tubular DE actuators are less bulky and more versatile for applications (Cameron et al., 2008; Stoyanov et al., 2008; Zhu, Stoyanov, Kofod, & Suo, 2010).

Instability analysis for DE devices is of considerable theoretical and industrial significance. However, the coupled partial differential equations governing the wrinkling behavior of DEs are difficult to solve, even numerically, due to geometric/physical non-linearities and multi-physics coupling. Robust numerical strategies should be developed for solving the resulting dispersion equations.

From a practical viewpoint, DEs may suffer from more failure modes than purely elastic elastomers, such as pull-in (snap-through) instability (Pelrine, Kornbluh, Pei, & Joseph, 2000; Zhao & Suo, 2007; Zurlo, Destrade, DeTommasi, & Puglisi, 2017), electric breakdown (Dissado & Fothergill, 1992; Stark & Garton, 1955; Zhang et al., 2017), buckling instability (Bertoldi & Gei, 2011; Gei, Colonnelli, & Springhetti, 2014; Goshkoderia & Rudykh, 2017), localized necking (Fu, Dorfmann, & Xie, 2018a; Fu, Xie, & Dorfmann, 2018b) and bulging (Che, Lu, & Wang, 2017; Lu, An, Li, Yuan, & Wang, 2015; Wang, Yuan, Lu, & Wang, 2017), which pose clear limitations on developing DE devices. Moreover, there are complicated transitions and competitions between these failure modes, and thus a comprehensive comparison is required for reliability analysis.

On the other hand, these instability modes can be seen as beneficial: hence, the electromechanical coupling behavior of DEs can generate complex 3D patterns, useful to control surface shapes (Pang et al., 2020; Wang, Gossweiler, Craig, & Zhao, 2014); similarly, the large actuation induced by the pull-in instability is eagerly pursued in DE actuators to produce giant changes in surface area (Huang et al., 2012).

Compared with planar DE devices, instability analysis in tubular devices is complicated by geometrical complexity and finite deformation inhomogeneity. Singh (1966) first studied the static response of a DE tube under radial electric field. Dorfmann and Ogden (2005, 2006) investigated the azimuthal shear, extension and inflation responses of a DE tube subject to a radial electric field. Later, they specialized the boundary value problem to the Gent dielectric model in a review article (Dorfmann & Ogden, 2017) to illustrate numerically the influence of the applied electric field on the deformation of the tube. Zhu et al. (2010) studied the finite deformation of a pre-stressed DE tube and analyzed the snap-through instability using the so-called Hessian approach. They indicated that it can be enhanced by applying pre-stress along the length. Note that the Hessian approach cannot predict inhomogeneous wrinkling-type instabilities, which requires incremental analysis. Shmuel and deBotton (2013) and Wu, Su, Chen, and Zhang (2017) studied axisymmetric and circumferential waves in a finitely deformed DE tube subject to a radial voltage, respectively. Note that the vanishing of the wave speed corresponds to the threshold of wrinkling instability. Su, Zhou, Chen, and Lü (2016a); Su, Wang, Zhang, and Chen (2016b) examined non-axisymmetric waves and the wrinkling instability of an incompressible DE tube. They obtained analytical dispersion equations in terms of Bessel functions by assuming a homogeneous finite pre-deformation. Bortot and Shmuel (2018) and Melnikov and Ogden (2018) studied the prismatic and axisymmetric 2D wrinkling of a DE tube subject to a radial voltage and an axial pre-stretch. Lu et al. (2015) investigated electromechanical bulging instability in a finitely deformed DE tube. They obtained the equilibrium and stability governing equations from the first and second variations of the free energy of the thermodynamic system. Their tube is considered thin and the mechanical and electric fields are assumed to be homogeneous to simplify the analysis.

With this paper, we propose a theoretical analysis of finite deformation and the associated 3D wrinkling-type instability (or buckling) of an incompressible DE tube subject to the combined action of a radial electrical voltage and mechanical loads. We consider not only the *wrinkling instability*, but also the instabilities due to *pull-in* (snap-through) and to *electric breakdown*, and examine the transition and competition between these failures. Additionally, we study the effect of actuation methods on the nonlinear response and the stability of the tube.

The originality and innovative aspects of the current paper include

- Presenting a *3D wrinkling analysis* for a DE tube subject to a radially inhomogeneous electric field, an axial force (or stretch), and twisting moments applied at the top and bottom faces. Here we note that most of the existing work so far is concerned with 2D wrinkling instability of DE tubes, while a 3D analysis reveals more information about the various modes actually selected in the instability process, especially for a tube with finite length.
- Investigating the *extensional wrinkling mode* in a stretched DE tube, which does not occur in purely elastic solids with Mooney-Rivlin or neoHookean strain energy. So far only contractile wrinkling has been considered for DE tubes and not the extensional wrinkling mode, which may occur in stretched DE films, see Fig. 1 and Su, Broderick, Chen, and Destrade (2018).
- Revealing the *competitive effects* between voltage and mechanical loadings, and investigating the influence of *actuation method* on the finite deformation and instabilities of the tube.
- Investigating the *transition and competitive mechanism between failure modes* in a DE tube. Instabilities in DE elastomers have been well investigated. Here we find scenarios where one instability triggers another, and propose a rational approach for designing stable structural patterns on demand and obtaining stable large actuation deformations of DE tubes.

The paper is structured as follows. In Section 2, we derive the governing equations for a finitely deformed DE tube subject to a radial voltage, internal pressure, an axial pre-stretch and a torsion, based on the nonlinear theory of electro-elasticity developed by Dorfmann and Ogden (2005, 2016). Note that there are some other electroelasitc models proposed, for example, by Yang and Hu (2004), Romeo (2011), Poya et al. (2018), etc. We then formulate the linearized incremental equations of motion in Section 3. To solve the incremental boundary value problem, we use the surface impedance matrix method, a robust numerical procedure for deriving the threshold for the onset of the instability.

In Section 4, we illustrate the actuation methods of the tube and specialize the formulas obtained in Sections 2 and 3 to *ideal Mooney-Rivlin* dielectric models. Here two problems corresponding to two different loading paths are considered. In the
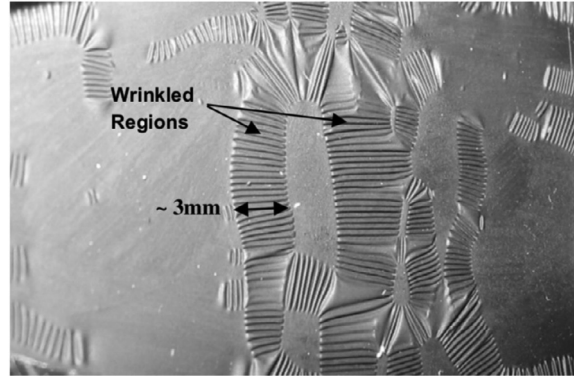
Fig. 1. Wrinkles in a stretched DE film, which may occur before or during the snap-through instability (Plante & Dubowsky, 2006).

first problem, the tube is subject to a fixed radial voltage and a torsion where the top and bottom ends of the tube move under the action of an axial force *F*: the *force-tuning problem*. In the second problem, the tube is subject to a fixed axial pre-stretch, a torsion created by moments applied at the top and bottom faces and a variable radial voltage: the *voltage-tuning problem*.

The numerical analysis for each problem is detailed in Sections 5 and 6, respectively, where the influences of actuation methods, geometrical parameters of the tube, electric field and mechanical loading on the transition and competition of instabilities are investigated. Moreover, we find the condition for the occurrence of extensional buckling in the solid. Finally in Section 7, we draw some conclusions.

2. Finite deformation of a DE tube

Consider an isotropic, incompressible DE tube with initial length *L*, inner radius R_i and outer radius R_o, respectively, as illustrated in Fig. 2(a). Here and thereafter, the physical parameters at the inner and outer faces of the tube are indicated with the subscripts '*i*' and '*o*', respectively. The inner and outer faces of the tube are covered with two flexible electrodes (carbon grease for example), which don't play a mechanical role during the deformation.

Using the referential cylindrical system (R, Θ, Z), a material particle in the undeformed configuration is labeled by its position vector $\boldsymbol{X}(R, \Theta, Z)$. The dimensionless lengths $\bar{R}_o = R_o/R_i$ and $\bar{L} = L/H$ are adopted to denote the initial radius and length aspect ratios, respectively, where $H = R_o - R_i$ is the undeformed thickness of the tube.

The DE tube deforms finitely, subject to the combined action of a voltage *V* across the thickness, an internal pressure *P* on the inner face, a mechanical load *F* along the length and a torsion at the two faces of the tube with closed ends. Using the current cylindrical system (r, θ, z), the material particle $\boldsymbol{X}$ takes up the position $\boldsymbol{x}(r, \theta, z)$ in the deformed configuration. Taking incompressibility of the material into account, the deformation is given by Ogden (1997)

$$R^2 - R_i^2 = \lambda_z(r^2 - r_i^2), \qquad \theta = \Theta + \gamma \lambda_z Z, \qquad z = \lambda_z Z, \tag{1}$$

where γ is the torsion angle per unit length (the twist), λ_z is the uniform axial stretch of the tube, r_i and r_o are inner and outer radii of the deformed tube, respectively. The length and thickness of the deformed tube are $l = \lambda_z L$ and $h = r_o - r_i$, respectively, as depicted in Fig. 2(b).

Then the deformation gradient $\boldsymbol{F} = \partial \boldsymbol{x}/\partial \boldsymbol{X}$ reads

$$\boldsymbol{F} = \begin{bmatrix} \partial r/\partial R & (1/R)\partial r/\partial \Theta & \partial r/\partial Z \\ r\partial \theta/\partial R & (r/R)\partial \theta/\partial \Theta & r\partial \theta/\partial Z \\ \partial z/\partial R & (1/R)\partial z/\partial \Theta & \partial z/\partial Z \end{bmatrix} = \begin{bmatrix} \lambda^{-1}\lambda_z^{-1} & 0 & 0 \\ 0 & \lambda & \gamma \lambda_z r \\ 0 & 0 & \lambda_z \end{bmatrix}, \tag{2}$$

where $\lambda = r/R$ is the *circumferential stretch*. Note that due to the material incompressibility constraint we have $\det \boldsymbol{F} = 1$, so that the imposed deformation is volume preserving.

From Eq. (1), we establish the following relationship between the circumferential stretches at the inner and outer surfaces $\lambda_i = r_i/R_i$ and $\lambda_o = r_o/R_o$ and the axial stretch λ_z of the deformed tube,

$$\lambda_o = \frac{1}{\bar{R}_o}\sqrt{\frac{1}{\lambda_z}\left(\bar{R}_o^2 + \lambda_z\lambda_i^2 - 1\right)}. \tag{3}$$

The deformed radial ratio is derived as

$$\bar{r}_o = \frac{r_o}{r_i} = \frac{\lambda_o \bar{R}_o}{\lambda_i}, \tag{4}$$
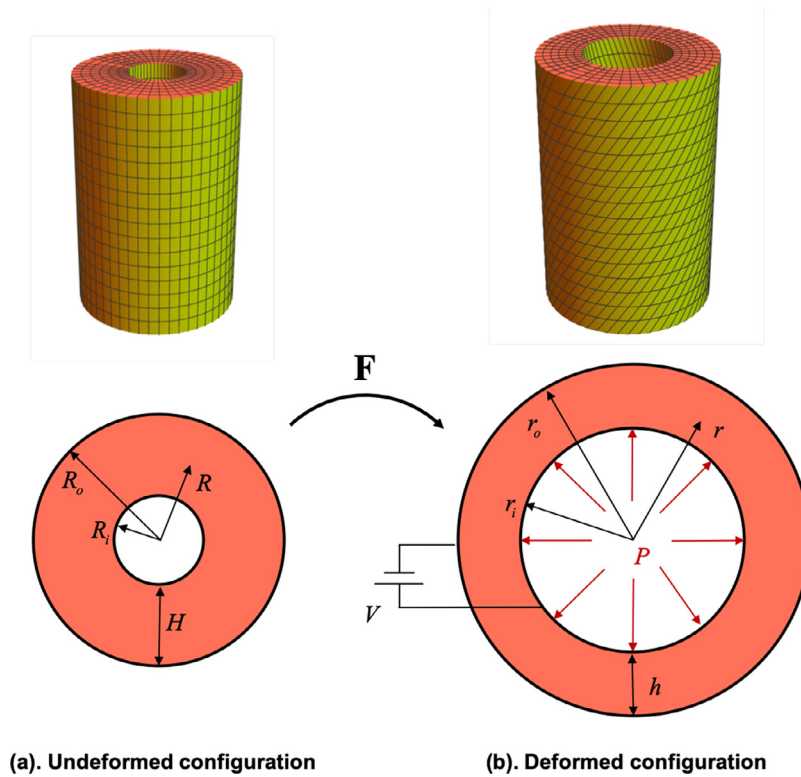
Fig. 2. Sketch of a DE tube in the (a) undeformed and (b) deformed configurations. The upper row presents three dimensional images of the tubes and the lower row shows the associated in-plane cross sections.

and the ratio of the inner volume of the deformed tube to that in the undeformed configuration is

$$\overline{\Delta} = \lambda_i^2 \lambda_z. \tag{5}$$

For this problem, the nominal electric field and the electric displacement vectors are

$$\boldsymbol{E}_l = \begin{bmatrix} E_R & 0 & 0 \end{bmatrix}^{\mathrm{T}}, \qquad \boldsymbol{D}_l = \begin{bmatrix} D_R & 0 & 0 \end{bmatrix}^{\mathrm{T}}, \tag{6}$$

where E_R and D_R are the only non-zero components of the nominal electric field and electric displacement, respectively. Then the true electric field and electric displacement in the deformed configuration can be obtained as

$$\boldsymbol{E} = \boldsymbol{F}^{-T}\boldsymbol{E}_l = \begin{bmatrix} E_r & 0 & 0 \end{bmatrix}^{\mathrm{T}}, \qquad \boldsymbol{D} = \boldsymbol{F}\boldsymbol{D}_l = \begin{bmatrix} D_r & 0 & 0 \end{bmatrix}^{\mathrm{T}}, \tag{7}$$

where $E_r = \lambda \lambda_z E_R$ and $D_r = \lambda^{-1}\lambda_z^{-1}D_R$, according to Eqs. (2) and (6).

The Maxwell equation reads

$$\mathrm{div}\boldsymbol{D} = \frac{1}{r}\frac{\partial (rD_r)}{\partial r} = 0, \tag{8}$$

here, so that rD_r is a constant.

According to the nonlinear electroelasticity (Dorfmann & Ogden, 2005; 2006), the nominal electric field is obtained as

$$E_R = \frac{\partial W}{\partial D_R}, \tag{9}$$

where $W = W(\lambda, \lambda_z, D_R)$ is a reduced energy function.

Finally, the applied voltage is

$$V = \int_{r_i}^{r_o} E_r \, \mathrm{d}r = \int_{r_i}^{r_o} \lambda \lambda_z \frac{\partial W}{\partial D_R} \, \mathrm{d}r. \tag{10}$$

On the other hand, the non-zero components of the Cauchy stress are (Su, Wu, Chen, & Destrade, 2019)

$$\tau_{rr} = 2\lambda^{-2}\lambda_z^{-2}\Omega_1 - 2\lambda^2\lambda_z^2\Omega_2 + 2\lambda^{-2}\lambda_z^{-2}D_R^2\Omega_5 + 4\lambda^{-4}\lambda_z^{-4}D_R^2\Omega_6 - q,$$

$$\tau_{\theta\theta} = 2(\lambda^2 + \gamma^2\lambda_z^2 r^2)\Omega_1 - 2\lambda^{-2}\Omega_2 - q,$$

$$\tau_{zz} = 2\lambda_z^2 \Omega_1 - 2\left(\lambda_z^{-2} + \gamma^2 \lambda^{-2} r^2\right)\Omega_2 - q,$$

$$\tau_{\theta z} = \tau_{z\theta} = 2\gamma r\left(\lambda_z^2 \Omega_1 + \lambda^{-2}\Omega_2\right), \tag{11}$$

where $\Omega_i = \partial \Omega / \partial I_i$ $(i = 1, 2, 4, 5, 6)$, Ω is the energy function of the solid which can be expressed in terms of the following five invariants

$$I_1 = \mathrm{tr}\boldsymbol{c}, \quad I_2 = \mathrm{tr}\left(\boldsymbol{c}^{-1}\right), \quad I_4 = \boldsymbol{D}_l \cdot \boldsymbol{D}_l, \quad I_5 = \boldsymbol{D}_l \cdot \boldsymbol{c}\boldsymbol{D}_l, \quad I_6 = \boldsymbol{D}_l \cdot \boldsymbol{c}^2\boldsymbol{D}_l, \tag{12}$$

with $\boldsymbol{c} = \boldsymbol{F}^{\mathrm{T}}\boldsymbol{F}$ being the right Cauchy-Green deformation tensor,

$$q = p - 2\Omega_2, \tag{13}$$

with p being a Lagrange multiplier associated with the incompressibility constraint, to be determined from the equilibrium equations and boundary conditions.

The equations of equilibrium reduce to

$$\frac{\partial \tau_{rr}}{\partial r} + \frac{1}{r}\left(\tau_{rr} - \tau_{\theta\theta}\right) = 0. \tag{14}$$

Using Eq. (14) and the boundary conditions $\tau_{rr}(r_i) = -P$ and $\tau_{rr}(r_o) = 0$, the relation between λ_i, λ_o and V can be established as

$$P = \int_{r_i}^{r_o} (\tau_{\theta\theta} - \tau_{rr}) \frac{\mathrm{d}r}{r} = \int_{\lambda_i}^{\lambda_o} \frac{\tau_{\theta\theta} - \tau_{rr}}{\lambda(1 - \lambda_z\lambda^2)} \, \mathrm{d}\lambda. \tag{15}$$

Here the relationship

$$\frac{\mathrm{d}r}{r} = \frac{\mathrm{d}\lambda}{\lambda\left(1 - \lambda_z\lambda^2\right)}, \tag{16}$$

has been used, which results from Eq. (1). The expression of the applied voltage V can be obtained by combining Eqs. (10) and (15).

The radial stress τ_{rr} is obtained as

$$\tau_{rr} = \int_{\lambda_i}^{\lambda} \frac{\tau_{\theta\theta} - \tau_{rr}}{\lambda(1 - \lambda_z\lambda^2)} \, \mathrm{d}\lambda - P. \tag{17}$$

As a result, the full stress distribution in the deformed tube can be determined from Eq. (11). The axial mechanical load applied at the end of the tube follows as

$$F = 2\pi \int_{r_i}^{r_o} \tau_{zz} r \, \mathrm{d}r - \pi r_i^2 P. \tag{18}$$

Finally, the nonlinear response of the DE tube can be determined by solving the above equations.

3. Linearized stability analysis

An extremely deformed dielectric may eventually buckle, a phenomenon which can be modelled by a linearized incremental wrinkling analysis (Bertoldi & Gei, 2011; Bortot & Shmuel, 2018; Goshkoderia & Rudykh, 2017; Melnikov & Ogden, 2018; Su et al., 2019). Hence, superimpose a 3D small harmonic inhomogeneous incremental deformation $\boldsymbol{u} = \boldsymbol{u}(\boldsymbol{x})$ along with an incremental electric displacement $\dot{\boldsymbol{D}}_l$ in the deformed configuration of the tube, with components in the form

$$u_i = u_i(r, \theta, z), \qquad \dot{D}_{l0i} = \dot{D}_{l0i}(r, \theta, z) \qquad i = r, \theta, z. \tag{19}$$

Hereinafter, incremental quantities are identified by a superimposed dot.

The governing equations are the incremental equations of equilibrium

$$\mathrm{div}\dot{\boldsymbol{T}} = \boldsymbol{0}, \qquad \mathrm{div}\dot{\boldsymbol{D}} = 0, \qquad \mathrm{curl}\dot{\boldsymbol{E}} = 0, \tag{20}$$

and of incompressibility

$$\mathrm{div}\boldsymbol{u} = 0, \tag{21}$$

where $\dot{\boldsymbol{T}}$ and $\dot{\boldsymbol{E}}$ are push-forward forms of incremental Cauchy stress and incremental electric filed, respectively. They can be written as (Dorfmann & Ogden, 2016)

$$\dot{\boldsymbol{T}} = \mathcal{A}(\mathrm{grad}\boldsymbol{u}) + \boldsymbol{\Gamma}\dot{\boldsymbol{D}} + p(\mathrm{grad}\boldsymbol{u}) - \dot{p}\boldsymbol{I}, \qquad \dot{\boldsymbol{E}} = \boldsymbol{\Gamma}^T(\mathrm{grad}\boldsymbol{u}) + \boldsymbol{K}\dot{\boldsymbol{D}}, \tag{22}$$

where the fourth-, third- and second-order tensors $\mathcal{A}$, $\boldsymbol{\Gamma}$ and $\boldsymbol{K}$ are the effective electroelastic moduli, with Cartesian components

$$\mathcal{A}_{piqj} = \mathcal{A}_{qjpi} = F_{p\alpha}F_{q\beta}\frac{\partial^2 \tilde{\Omega}}{\partial F_{i\alpha} \partial F_{j\beta}}, \qquad \Gamma_{piq} = \Gamma_{ipq} = F_{p\alpha}F_{\beta q}^{-1}\frac{\partial^2 \tilde{\Omega}}{\partial F_{i\alpha} \partial D_{l\beta}},$$

$$K_{ij} = K_{ji} = F_{\alpha i}^{-1} F_{\beta j}^{-1} \frac{\partial^2 \tilde{\Omega}}{\partial D_{l\alpha} \partial D_{l\beta}}. \tag{23}$$

Here, $\tilde{\Omega} = \tilde{\Omega}(\boldsymbol{F}, \boldsymbol{D}_l) = \Omega(I_1, I_2, I_4, I_5, I_6)$ is the augmented free energy function. The non-zero components of the electro-elastic moduli with respect to the specific deformation gradient (2) for ideal dielectrics (Section 4.2.1) are listed in Appendix A.

According to Eq. (20)$_3$, the incremental electric field can be expressed as $\dot{\boldsymbol{E}} = -\mathrm{grad}\dot{\phi}$, where $\dot{\phi}$ is an incremental electric potential.

The solutions of the incremental problem can be expanded in series in the form

$$u_r = \sum_{n=0}^{\infty} U_r(r)\mathrm{e}^{\mathrm{i}(n\theta+kz)}, \quad u_\theta = \sum_{n=0}^{\infty} U_\theta(r)\mathrm{e}^{\mathrm{i}(n\theta+kz)},$$

$$u_z = \sum_{n=0}^{\infty} U_z(r)\mathrm{e}^{\mathrm{i}(n\theta+kz)}, \quad \dot{\phi} = \sum_{n=0}^{\infty} \Phi(r)\mathrm{e}^{\mathrm{i}(n\theta+kz)},$$

$$\dot{T}_{rr} = \sum_{n=0}^{\infty} \Sigma_{rr}(r)\mathrm{e}^{\mathrm{i}(n\theta+kz)}, \quad \dot{T}_{r\theta} = \sum_{n=0}^{\infty} \Sigma_{r\theta}(r)\mathrm{e}^{\mathrm{i}(n\theta+kz)},$$

$$\dot{T}_{rz} = \sum_{n=0}^{\infty} \Sigma_{rz}(r)\mathrm{e}^{\mathrm{i}(n\theta+kz)}, \quad \dot{D}_r = \sum_{n=0}^{\infty} \Delta_r(r)\mathrm{e}^{\mathrm{i}(n\theta+kz)}, \tag{24}$$

where U_r, U_θ, U_z, Φ, Σ_{rr}, $\Sigma_{r\theta}$, Σ_{rz} and Δ_r are scalar functions of r only, $n = 0, 1, 2 \ldots$ is the *circumferential wavenumber*, and k is the *axial wavenumber*, which can be connected to the length L using the lateral incremental boundary condition at the ends of the tube $z = 0, \ell$.

The incremental boundary conditions on the curved faces $r = r_i$ and $r = r_o$ read, respectively,

$$\dot{T}_{0rr} = P\frac{\partial u_r}{\partial r} + \dot{P}, \quad \dot{T}_{0r\theta} = \frac{P}{r}\left(\frac{\partial u_r}{\partial \theta} - u_\theta\right), \quad \dot{T}_{0rz} = P\frac{\partial u_r}{\partial z}, \quad \dot{\phi} = 0, \tag{25}$$

and

$$\dot{T}_{0rr} = \dot{T}_{0r\theta} = \dot{T}_{0rz} = \dot{\phi} = 0, \tag{26}$$

where P is a prescribed constant thus $\dot{P} \equiv 0$.

To solve this boundary value problem, we use the *surface impedance matrix method* to build a robust numerical procedure.

First, the incremental governing Eqs. (20)–(22) are recast in the form of a first-order differential system (Destrade, Annaidh, & Coman, 2009; Su et al., 2019),

$$\frac{\mathrm{d}}{\mathrm{d}r}\boldsymbol{\eta}(r) = \frac{\mathrm{i}}{r}\begin{bmatrix} \boldsymbol{G}^a & \boldsymbol{G}^b \\ \boldsymbol{G}^c & (\boldsymbol{G}^a)^\dagger \end{bmatrix}\boldsymbol{\eta}(r), \tag{27}$$

where † denotes the Hermitian operator,[1] and

$$\boldsymbol{\eta}(r) = \begin{bmatrix} U_r & U_\theta & U_z & \mathrm{i}r\Delta_r & \mathrm{i}r\Sigma_{rr} & \mathrm{i}r\Sigma_{r\theta} & \mathrm{i}r\Sigma_{rz} & \Phi \end{bmatrix}^\mathrm{T} = \begin{bmatrix} \boldsymbol{U} & \boldsymbol{S} \end{bmatrix}^\mathrm{T}, \tag{28}$$

is the Stroh vector, and $\boldsymbol{U} = \begin{bmatrix} U_r & U_\theta & U_z & \mathrm{i}r\Delta_r \end{bmatrix}^\mathrm{T}$, $\boldsymbol{S} = \begin{bmatrix} \mathrm{i}r\Sigma_{rr} & \mathrm{i}r\Sigma_{\mathrm{i}r\theta} & \mathrm{i}r\Sigma_{rz} & \Phi \end{bmatrix}^\mathrm{T}$ are the generalized displacement and traction vectors, respectively. The derivation of Eq. (27) and the components of the 4×4 submatrixes $\boldsymbol{G}_a$, $\boldsymbol{G}_b$ and $\boldsymbol{G}_c$ are given in Appendix B for reference. Note that the orthogonality of trigonometric functions have been used to derive Eq. (28).

Now the incremental boundary conditions (25) and (26) read, respectively,

$$\boldsymbol{S}(r_i) = P\begin{bmatrix} -1 & -n & -kr & 0 \\ -n & -1/r & 0 & 0 \\ -kr & 0 & 0 & 0 \\ 0 & 0 & 0 & 0 \end{bmatrix}\boldsymbol{U}(r_i), \tag{29}$$

and

$$\boldsymbol{S}(r_o) = \boldsymbol{0}. \tag{30}$$

---

[1] A simple example for a 2×2 matrix:

$$\begin{bmatrix} a_1 & \mathrm{i}a_2 \\ a_3 & \mathrm{i}a_4 \end{bmatrix}^\dagger = \begin{bmatrix} a_1 & a_3 \\ -\mathrm{i}a_2 & -\mathrm{i}a_4 \end{bmatrix},$$

where $a_1 - a_4$ are real numbers.

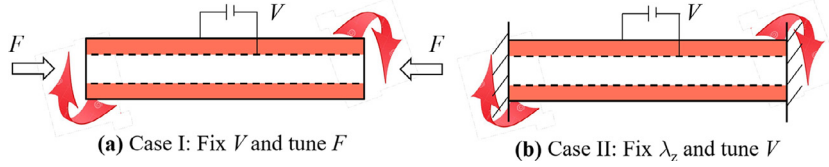**(a)** Case I: Fix V and tune F **(b)** Case II: Fix λ_z and tune V

Fig. 3. DE tubes coated with two compliant electrodes on the inner and outer faces activated by different loading protocols.

Then, define the so-called conditional impedance matrix $\boldsymbol{z}^i(r, r_i)$, linking the traction and the displacement vectors as

$$\boldsymbol{S}(r) = \boldsymbol{z}^i(r, r_i)\boldsymbol{U}(r). \tag{31}$$

Substituting Eq. (31) into Eq. (27), and eliminating $\boldsymbol{U}$, gives a Riccati differential equation for $\boldsymbol{z}^i$,

$$\frac{\mathrm{d}\boldsymbol{z}^i}{\mathrm{d}r} = \frac{1}{r}\left[-\mathrm{i}\boldsymbol{z}^i\boldsymbol{G}^a + \boldsymbol{z}^i\boldsymbol{G}^b\boldsymbol{z}^i + \boldsymbol{G}^c + \mathrm{i}(\boldsymbol{G}^a)^\dagger\boldsymbol{z}^i\right]. \tag{32}$$

Now integrate Eq. (32) from r_i to r_o, with the following initial and stop conditions derived by combining Eqs. (29)–(31),

$$\boldsymbol{z}^i(r_i, r_i) = P\begin{bmatrix} -1 & -n & -kr & 0 \\ -n & -1/r & 0 & 0 \\ -kr & 0 & 0 & 0 \\ 0 & 0 & 0 & 0 \end{bmatrix}, \qquad \det \boldsymbol{z}^i(r_o, r_i) = 0. \tag{33}$$

The wrinkling behavior of the tube is governed by Eqs. (32) and (33), from which the critical axial stretch for the onset of instability is found numerically,

$$\lambda_z^c = \lambda_z^c(k, n; \bar{R}_o, V, \gamma), \tag{34}$$

for given wavenumber k, buckling mode n (the number of circumferential wrinkles), radius ratio $\bar{R}_o$, voltage V and twist γ.

Once Eq. (32) is solved, the ratios of the incremental displacements on the outer face of the tube $t_\theta = U_\theta(r_o)/U_r(r_o)$, $t_z = U_z(r_o)/U_r(r_o)$, $t_\Phi = \Phi(r_o)/U_r(r_o)$ follow from $\boldsymbol{S}(r_o) = \boldsymbol{z}^i(r_o, r_i)\boldsymbol{U}(r_o) = \boldsymbol{0}$. These give the wrinkling shape on the outer face of the tube. To obtain the through-thickness displacement fields in the tube, we integrate another Riccati equation,

$$\frac{\mathrm{d}\boldsymbol{z}^o}{\mathrm{d}r} = \frac{1}{r}\left[-\mathrm{i}\boldsymbol{z}^o\boldsymbol{G}^a + \boldsymbol{z}^o\boldsymbol{G}^b\boldsymbol{z}^o + \boldsymbol{G}^c + \mathrm{i}(\boldsymbol{G}^a)^\dagger\boldsymbol{z}^o\right]. \tag{35}$$

from the outer $r = r_o$ to the inner face $r = r_i$, this time for the other conditional impedance matrix $\boldsymbol{z}^o(r, r_o)$, which is such that

$$\boldsymbol{S}(r) = \boldsymbol{z}^o(r, r_o)\boldsymbol{U}(r). \tag{36}$$

Now the full distribution of the incremental field $\boldsymbol{U}$ and the corresponding buckling pattern of the tube can be obtained by a simultaneous numerical integrations of Eq. (35) and the first of Eq. (27), i.e.

$$\frac{\mathrm{d}}{\mathrm{d}r}\boldsymbol{U} = \frac{\mathrm{i}}{r}\boldsymbol{G}^a\boldsymbol{U} - \frac{1}{r}\boldsymbol{G}^b\boldsymbol{z}^o\boldsymbol{U}, \tag{37}$$

from r_o to r_i, with initial conditions

$$\boldsymbol{z}^o(r_o, r_o) = \boldsymbol{0}, \qquad \boldsymbol{U}(r_o) = U(r_o)\begin{bmatrix} 1 & t_\theta & t_z & t_\Phi \end{bmatrix}^\mathrm{T}. \tag{38}$$

Here $U(r_o)$ is a constant, of an amplitude which cannot be determined by our linear stability analysis.

4. Loading methods and material model

4.1. Loading methods

In this section, we consider two different loading methods to activate the DE tube, see Fig. 3,

- *Problem I: Force Tuning.* The tube is subject to a fixed voltage V attached to its inner and outer faces, a fixed amount of torsion with twist γ and a varying axial force F.
- *Problem II: Voltage Tuning.* The tube is subject to a fixed axial constraint λ_z, a fixed amount of torsion with twist γ and a varying radial voltage V.

4.2. Material model

4.2.1. Ideal dielectric model

For the constitutive response of the DE tube, we consider the so-called *ideal dielectric elastomer*, with energy function of the form

$$\Omega = W(I_1, I_2) + \frac{\varepsilon}{2} I_5, \tag{39}$$

where ε is the permittivity of the solid, which is independent of deformation, W is derived from any isotropic purely elastic strain-energy function.

The true electric field in ideal dielectrics can be determined from Eqs. (8), (10) and (39) as

$$E_r = \frac{V}{\ln \bar{r}_o} \frac{1}{r}. \tag{40}$$

The dimensionless radial stress $\bar{\tau}_{rr} = \tau_{rr}/\mu$ is obtained from Eqs. (17) and (39) as

$$\bar{\tau}_{rr} = f(\lambda) - \bar{V}^2 g(\lambda) - \bar{P}, \tag{41}$$

where μ is the shear modulus of the solid in the absence of voltage and

$$f(\lambda) = \left(\overline{\Omega}_1 \lambda_z^{-2} + \overline{\Omega}_2\right)\left(\lambda^{-2} - \lambda_i^{-2}\right) - 2\left(\overline{\Omega}_1 \lambda_z^{-1} + \overline{\Omega}_2 \lambda_z\right) \ln \frac{\lambda}{\lambda_i} + \frac{\overline{\Omega}_1 \bar{\gamma}^2 \lambda_z^2 \left(\lambda^2 - \lambda_i^2\right)}{\bar{L}^2 \left(\bar{R}_o - 1\right)^2 \left(1 - \lambda_z \lambda^2\right)},$$

$$g(\lambda) = \frac{1}{2}\left(\frac{\bar{R}_o - 1}{\ln \bar{r}_o}\right)^2 \left[\frac{1}{\lambda_i^2} - \frac{\lambda_z \lambda^2 - 1}{\lambda^2\left(\lambda_z \lambda_i^2 - 1\right)}\right]. \tag{42}$$

In Eqs. (41) and (42) the following non-dimensional quantities have been used

$$\bar{V} = \frac{V}{H}\sqrt{\frac{\varepsilon}{\mu}}, \quad \bar{\gamma} = \gamma L, \quad \bar{P} = \frac{P}{\mu}, \quad \overline{\Omega}_i = \frac{\Omega_i}{\mu} \quad (i = 1, 2), \quad \overline{\Omega}_5 = \frac{\Omega_5}{\varepsilon}. \tag{43}$$

Then the dimensionless circumferential and axial stresses $\bar{\tau}_{\theta\theta} = \tau_{\theta\theta}/\mu$ and $\bar{\tau}_{zz} = \tau_{zz}/\mu$ follow from Eqs. (11) and (39). Using Eq. (41) and the boundary condition $\tau_{rr}(r_o) = 0$, the applied voltage can be expressed as

$$\bar{V} = \frac{\lambda_i \bar{r}_o \ln \bar{r}_o}{\bar{R}_o - 1}\sqrt{\frac{2f(\lambda_o) - 2\bar{P}}{\bar{r}_o^2 - 1}}. \tag{44}$$

4.2.2. Ideal Mooney-Rivlin dielectric model

For numerical illustration, we take the ideal Mooney-Rivlin dielectric elastomer with elastic energy density W given by Rivlin and Saunders (1951)

$$W(I_1, I_2) = \frac{c_1}{2}(I_1 - 3) + \frac{c_2}{2}(I_2 - 3), \tag{45}$$

where c_1, c_2 are positive material constants that satisfy the relationship $c_1 + c_2 = \mu$.

For convenience and some generality, we introduce the following dimensionless measures of the wavenumber, axial force, elastic parameters and electric field,

$$\bar{k} = k(R_o - R_i), \quad \bar{F} = \frac{F}{\pi\left(R_o^2 - R_i^2\right)},$$

$$\bar{c}_i = \frac{c_i}{\mu} \quad (i = 1, 2), \quad \bar{E}_r = E_r\sqrt{\frac{\varepsilon}{\mu}}. \tag{46}$$

For the ideal Mooney-Rivlin dielectric elastomer (45), we have

$$\overline{\Omega}_1 = \frac{\bar{c}_1}{2}, \quad \overline{\Omega}_2 = \frac{\bar{c}_2}{2}, \quad \overline{\Omega}_5 = \frac{1}{2}. \tag{47}$$

For our calculations, we use the material parameters $c_1 = 1.858 \times 10^5$ Pa, $c_2 = 0.1935 \times 10^5$ Pa (so that $\bar{c}_1 = 0.9$, $\bar{c}_2 = 0.1$) (Batra, Mueller, & Strehlow, 2005) and set the dimensionless breakdown electric field of the dielectric elastomer as $\bar{E}^B = E^B\sqrt{\varepsilon/\mu} = 2$ (Getz, Kochmann, & Shmuel, 2017), where E^B is the dielectric strength of the material.

In the following calculations, we set $\bar{P} \equiv 0$ and focus on the effects of the axial loading $\bar{F}$, radial voltage $\bar{V}$ and torsion $\bar{\gamma}$ on the nonlinear deformation and the instability behavior of the DE tube. The radius and length aspect ratios of the tube are taken to be $\bar{R}_o = 1.4$ and $\bar{L} = 6$, respectively, if not stated otherwise.
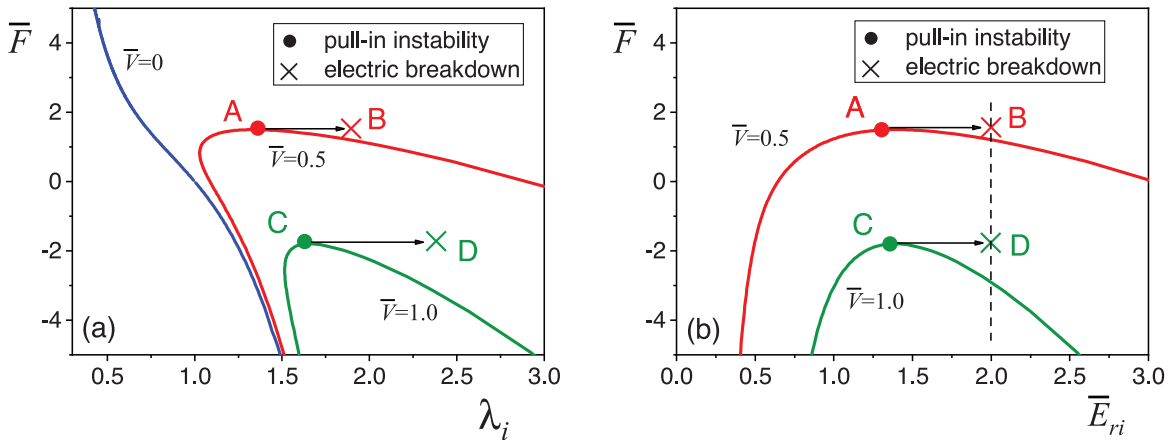
Fig. 4. Effect of the applied voltage $\overline{V}$ on the nonlinear responses of (a) inner circumferential stretch λ_i and (b) inner non-dimensional true electric field $\overline{E}_{ri}$ versus the axial stress $\overline{F}$ of a Mooney-Rivlin DE tube with $\overline{c}_1 = 0.9$, $\overline{\gamma} = 0$ and $\overline{R}_o = 1.4$ for Problem I-Force Tuning. The thresholds for pull-in instability and electric breakdown of the elastomer are marked by circles and crosses, respectively. The horizontal arrows represent the rapid stretch expected once the pull-in threshold is reached, until the electric breakdown.

5. Results for problem I: force tuning

5.1. Nonlinear response

Fig. 4 presents the nonlinear response of a Mooney-Rivlin DE tube with no torsion ($\overline{\gamma} = 0$) and an increasing series of fixed voltage $\overline{V} = 0.0, 0.5, 1.0$ subject to varying mechanical loadings $\overline{F}$ (Problem I). Both compressive ($\overline{F} < 0$) and tensile ($\overline{F} \geq 0$) loadings are considered.

In the purely elastic case $\overline{V} = 0$, the $\overline{F} - \lambda_i$ curve is monotonic: the tube shrinks circumferentially when subject to an axial extension, and expands circumferentially under axial compression.

With electromechanical coupling ($\overline{V} \neq 0$), the $\overline{F} - \lambda_i$ curve can become non-monotonic. The DE tube always expands circumferentially under axial compressive stress ($\overline{F} < 0$), and the response is independent of the applied voltage when the stress is sufficiently large, as all the curves superpose. On the other hand, the tube shrinks first and then expands as the axial stress increases ($\overline{F} > 0$). The physical mechanism behind the non-monotonic response of the tube can be understood as follows. In the early stages of the applied tensile stress, the mechanical loading dominates: the tube shrinks and the circumferential stretch decreases. As the stress increases, the tube thins, leading to an increase of the true electric field in the solid. Then the voltage plays a key role, making the tube expands as the circumferential stretch increases.

From Eq. (40) we note that $\overline{E}_{ri}$, the true electric field on the inner face, is always larger than $\overline{E}_{ro}$, the electric field on the outer face. Thus the solid fails by electric breakdown once $\overline{E}_{ri}$ exceeds the dielectric strength of the solid $\overline{E}^B = 2$. It can be seen that for tubes subject to a high electrical voltage, pull-in instability may occur in the solid as the load $\overline{F}$ reaches a critical value. In this case, the tube expands dramatically and will eventually fail by electric breakdown. This predicted sudden expansion of a DE tube subject to electromechanical loadings may provide a novel approach for designing large-volume fluid pumps (Wang et al., 2018).

Fig. 5 displays the nonlinear response of a Mooney-Rivlin DE tube for an increasing series of fixed torsion $\overline{\gamma} = 0.0, 0.7, 1.0$ and a fixed voltage $\overline{V} = 0.5$, subject to varying mechanical loadings $\overline{F}$ (Problem I). It can be observed that the application of torsion enhances the pull-in stability of the tube. When the applied torsion is sufficiently large, the pull-in instability of the tube can be suppressed (blue curve). Note that electric breakdown failure can happen prior to pull-in instability in a torsional tube (red curve).

5.2. Instability analysis

We plot the wrinkling dispersion curves in Fig. 6 for a Mooney-Rivlin DE tube with $\overline{c}_1 = 0.9$ and $\overline{R}_o = 1.4$ subject to an increasing voltage $\overline{V} = 0, 0.3, 0.6, 0.8$ and no torsion $\overline{\gamma} = 0$. Here we use the notation λ_z^V to denote the axial stretch of the tube induced by the voltage only (when $\overline{F} = 0, \overline{\gamma} = 0$).

First of all, we validate the analysis in Fig. 6(a) by recovering some known results for the buckling of a purely elastic tube by taking $\overline{V} = 0$ (Goriely, Vandiver, & Destrade, 2008). From Eq. (34), a series of dispersion branches can be obtained by taking $n = 0, 1, \ldots, 4$. We see that the tube is always stable in extension ($\lambda_z \geq \lambda_z^V = 1$), and can only buckle in contraction ($\lambda_z < \lambda_z^V$), once the stretch reaches the highest points of the $\lambda_z^c - \overline{k}$ curve, i.e., the bold black curve. For slender tubes with small $\overline{k}$, the Euler buckling mode $n = 1$ is dominant. As $\overline{k}$ increases, higher buckling modes can be induced, depending on
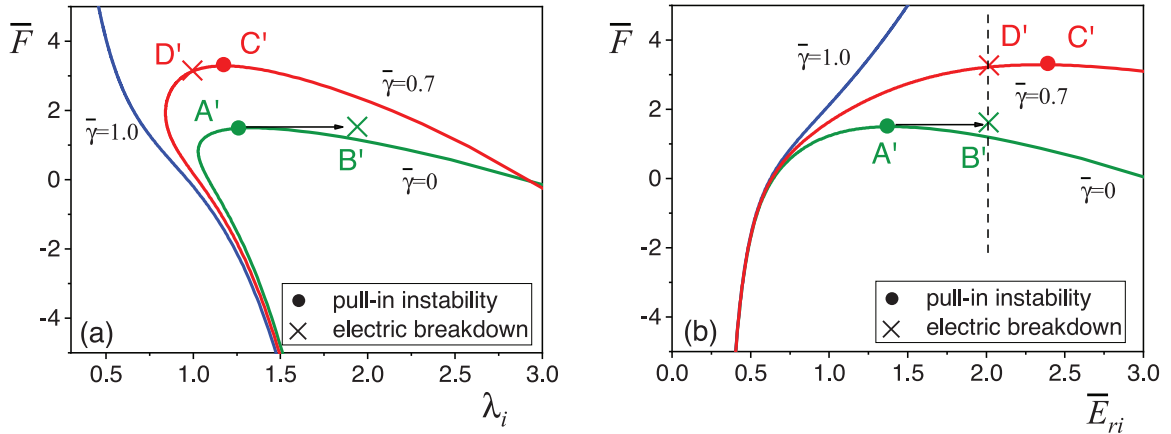
Fig. 5. Effect of the applied torsion $\overline{\gamma}$ on the nonlinear responses of (a) inner circumferential stretch λ_i and (b) inner non-dimensional true electric field $\overline{E}_{ri}$ versus the axial stress $\overline{F}$ of a Mooney-Rivlin DE tube with $\overline{c}_1 = 0.9$ and $\overline{R}_o = 1.4$ for Problem I-Force Tuning. The thresholds for pull-in instability and electric breakdown of the elastomer are marked by circles and crosses, respectively.
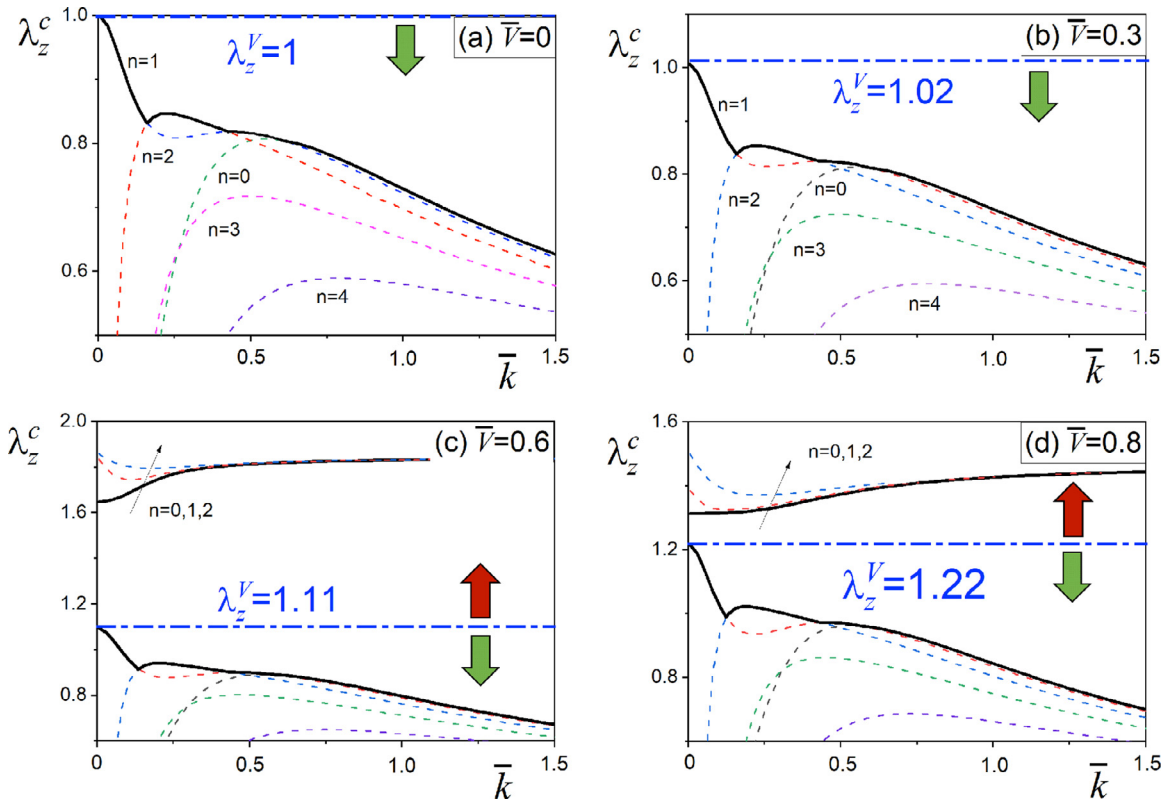
Fig. 6. Plots of the critical axial stretch λ_z^c versus the dimensionless axial wave number $\overline{k}$ for buckling of a voltage activated ($\overline{V} = 0, 0.3, 0.6, 0.8$) Mooney-Rivlin DE tube with $\overline{\gamma} = 0$, $\overline{c}_1 = 0.9$ and $\overline{R}_o = 1.4$ for a range of mode numbers $n = 0, 1, \ldots, 4$. (a) and (b): Subject to a low voltage, the tube can only buckle in contraction. (c) and (d): Subject to a higher voltage, the dielectric tube can buckle in extension as well, always in the $n = 0$ barrelling mode. The blue dot-dashed line denotes the axial stretch of the tube induced by the voltage only. (For interpretation of the references to color in this figure legend, the reader is referred to the web version of this article.)

the dimensions of the tube. For short and thick tubes with large $\overline{k}$, the first unstable mode is the first barrelling mode $n = 0$. The surface instability criterion of Biot for an elastic half-space is recovered as $\overline{k} \to +\infty$ (Biot, 1965).

For the case $\overline{V} = 0.3$, the solid can also only buckle in contraction. The tube expands axially to $\lambda_z^V > 1$ following the application of the voltage $\overline{V}$. Fixing the voltage and increasing the contraction, the solid buckles once the stretch reaches a critical value λ_z^c, depending on the wavenumber $\overline{k}$.
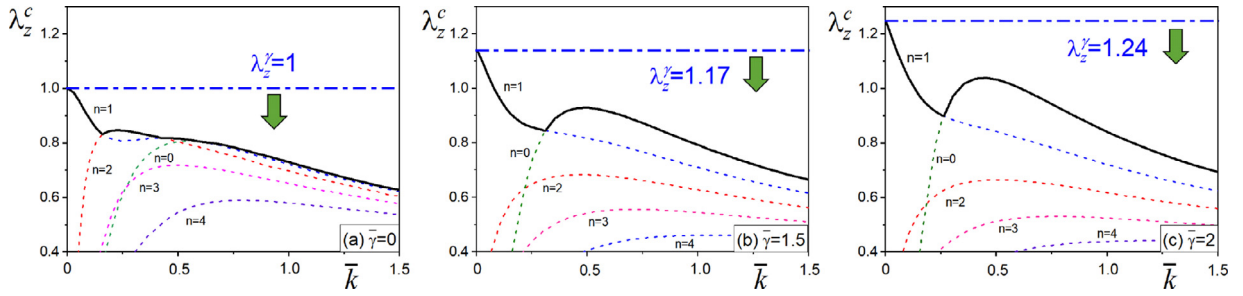
Fig. 7. Plots of the critical axial stretch λ_z^c versus the dimensionless axial wave number $\bar{k}$ for buckling of a Mooney-Rivlin DE tube with $\bar{c}_1 = 0.9$ and $\bar{R}_o = 1.4$ subject to no voltage ($\bar{V} = 0$) and a series of increased fixed amounts of torsion $\bar{\gamma} = 0.0, 1.5, 2.0$, for a range of mode numbers $n = 0, 1, \ldots, 4$. The blue dot-dashed line denotes the axial stretch of the tube induced by the torsion only. (For interpretation of the references to color in this figure legend, the reader is referred to the web version of this article.)
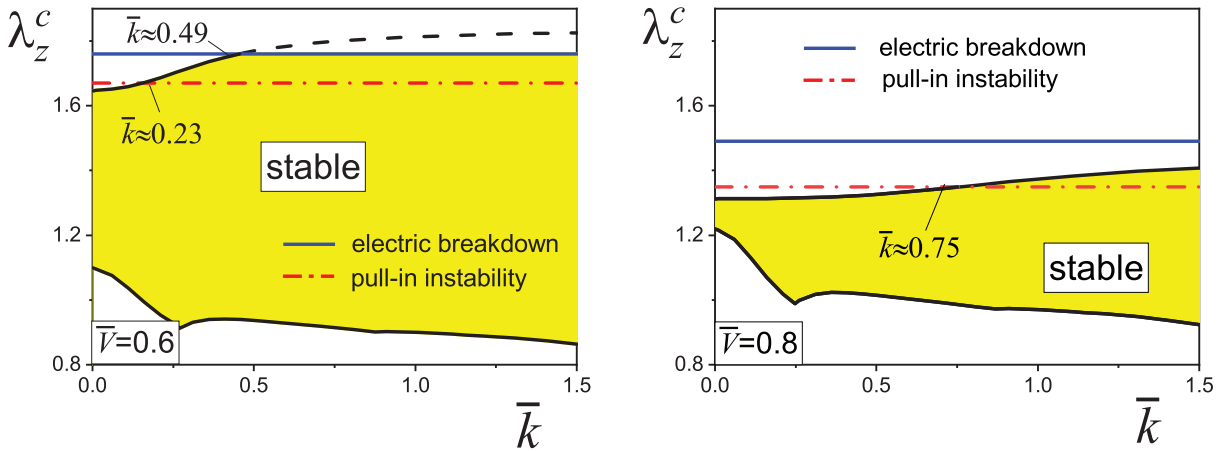
Fig. 8. Transition and competition between buckling, electric breakdown, and pull-in instabilities of Mooney-Rivlin DE tubes with $\bar{c}_1 = 0.9$ and $\bar{R}_o = 1.4$ subject to voltages $\bar{V} = 0.6, 0.8$. The red dot-dashed and blue solid lines correspond to the onsets of the pull-in instability and electric breakdown ($\bar{E}_{ri} = \bar{E}^B = 2$) of the tube, respectively. (For interpretation of the references to color in this figure legend, the reader is referred to the web version of this article.)

For the cases $\bar{V} = 0.6, 0.8$, we see that in addition to contractile buckling, the possibility of *buckling in extension* for the tube has now emerged (see Su et al. (2018) for this possibility in plane DE plates). Increasing the stretch of the tube beyond λ_z^V, the solid buckles once the stretch reaches the lowest point of the upper branches of the dispersion curves. It should be noted that the tube always buckles in the mode $n = 0$ when it is extremely stretched. The maximal allowable actuation decreases as the applied voltage increases.

In Fig. 7 we examine the effect of the torsion $\bar{\gamma}$ on the wrinkling dispersion curve for a Mooney-Rivlin DE tube with $\bar{c}_1 = 0.9$, $\bar{R}_o = 1.4$ and $\bar{V} = 0$. Here we use the notation λ_z^γ to denote the axial stretch of the tube induced by the torsion only (when $\bar{F} = 0, \bar{V} = 0$).

Due to the *Poynting effect*, an axially free tube ($\bar{F} = 0$) elongates to $\lambda_z^\gamma > 1$ once the torsion is applied. Fixing the torsion and sufficiently compressing the tube will buckle the structure (Ciarletta & Destrade, 2014). Observe here how the application of torsion suppresses higher mode buckling.

Fig. 8 presents the effect of the applied voltage $\bar{V}$ on instabilities transitions (buckling, electric breakdown and pull-in instability) in Mooney-Rivlin DE tubes with $\bar{c}_1 = 0.9$, $\bar{\gamma} = 0$ and $\bar{R}_o = 1.4$. Here only the meaningful $\lambda_z^c - \bar{k}$ curve is presented. Note that pull-in and electric breakdown do not occur in a compressed DE tube: we thus only consider the case of a stretched DE tube to look at the competition between the three instability modes.

When $\bar{V} = 0.6$ (figure on the left), we see that under a tensile axial force, buckling occurs first for slender tubes such that $\bar{k} \leq 0.23$. For thicker and stubbier tubes such that $\bar{k} \geq 0.49$, the tensile axial force stretches the tube safely until $\lambda_z^{max} \approx 1.66$ (red dot-dashed line), where the pull-in instability is triggered. Then the tube expands dramatically, with sudden decrease in thickness and increase in true electric field, until it fails by electric breakdown once $\bar{E}_{ri}$ reaches the threshold $\bar{E}_i^B = 2$. For tubes with $0.23 < \bar{k} < 0.49$, buckling occurs before electric breakdown in the tube, although it is transient and unstable.

When $\bar{V} = 0.8$ (figure on the right), buckling pattern occurs first in extension for slender tubes and also for shorter and thicker tubes, as long as $\bar{k} < 0.75$. Then for tubes such that $0.75 < \bar{k} < 1.5$, pull-in instability takes over and leads again to buckling instability, before failure by electric breakdown.
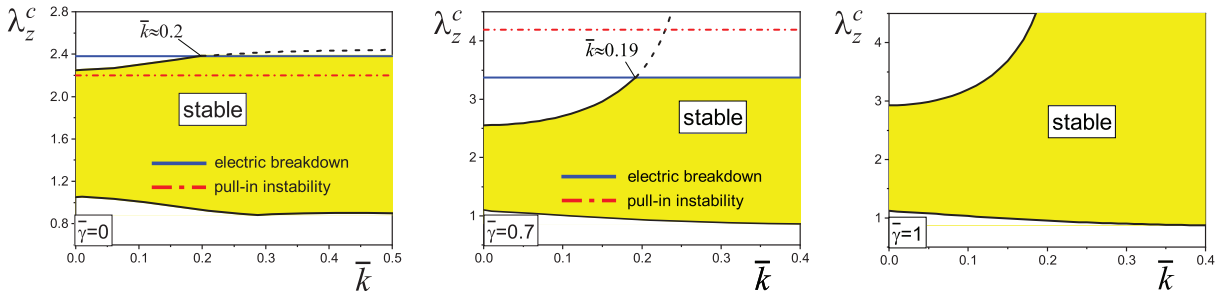
Fig. 9. Transition and competition between buckling, electric breakdown, and pull-in instabilities of Mooney-Rivlin DE tubes with $\bar{c}_1 = 0.9$ and $\bar{R}_o = 1.4$ subject to a fixed voltage $\bar{V} = 0.5$ and a varying torsion $\bar{\gamma} = 0, 0.7, 1$. The red dot-dashed and blue solid lines correspond to the onsets of the pull-in instability and electric breakdown ($\bar{E}_{ri} = \bar{E}^B = 2$) of the tube, respectively. (For interpretation of the references to color in this figure legend, the reader is referred to the web version of this article.)

Fig. 9 displays the effect of the applied torsion $\bar{\gamma}$ on instabilities transitions in Mooney-Rivlin DE tubes with $\bar{c}_1 = 0.9$ and $\bar{R}_o = 1.4$ subject a voltage $\bar{V} = 0.5$. When there is no torsion ($\bar{\gamma} = 0$), the pull-in instability will be triggered first as the axial stretch increases and the tube will fail by electric breakdown finally, which is consistent with the result presented in Fig. 5 (green curve). It can be seen that the application of a large torsion (e.g., $\bar{\gamma} = 0.7$) will make the electric breakdown failure occur first (see the red curve in Fig. 5). Increasing the torsion further (e.g., $\bar{\gamma} = 1.0$) can suppress the pull-in instability of the solid (see also the blue curve in Fig. 5). Note that applying torsion can not only suppress the pull-in instability, but also increase the threshold value for electric breakdown. As a result, the maximal allowable stretch of the tube can be increased. This observation may a provide a solid basis for designing high-performance DE sensors and actuators.

We now quantify better the concepts of slenderness and stubbiness, by linking $\bar{k}$ to the dimensions of the tube. We assume that the centre of the top face be directly aligned with that of the bottom face. This boundary condition can be achieved when (Ciarletta & Destrade, 2014)

$$\bar{k} = \frac{2m\pi}{\lambda_z} \frac{R_o - R_i}{L},$$

where the positive integer m is the number of the axial wrinkles.

Using Eq. (34) and the relationship (48), we plot in Fig. 10 the critical stretch and pattern shapes for buckling of DE tubes with specific radius and length aspect ratios $\bar{R}_o$ and $\bar{L}$ subject to a voltage $\bar{V}$ and a torsion $\bar{\gamma}$. In the purely elastic case ($\bar{V} = 0$, first four rows), the tube may only buckle in contraction. Here Cases (a), (c) and (d) show that increasing $\bar{L}$ or decreasing $\bar{R}_o$ destabilizes the solid. From Cases (a) and (b) we can see that the critical axial stretch increases as the applied torsion increases. Applying a voltage ($\bar{V} \neq 0$, last three rows) increases the critical stretch for contractile buckling and creates the possibility of extensional buckling. Note that the tube always buckles in a trumpet-shape ($m = 1$, $n = 0$) for buckling in extension. Various buckling modes can be designed on demand in a DE tube by finely tuning $\bar{V}$, $\bar{R}_o$, $\bar{\gamma}$ and $\bar{L}$.

6. Results for problem II: voltage tuning

6.1. Nonlinear response

Fig. 11 shows the nonlinear deformation of a Mooney-Rivlin DE tube with $\bar{c}_1 = 0.9$ and $\bar{R}_o = 1.4$ when the deformation is driven by voltage (Problem II). Here the $\bar{V} - \lambda_i$ curve is monotonic, and the pull-in instability of the solid is suppressed. The material eventually fails by electric breakdown at the inner face $r = r_i$ as the applied voltage reaches a critical value.

In Fig. 11(a), we consider the tube without torsion $\bar{\gamma} = 0$ and investigate the influence of axial pre-stretch λ_z on the deformation. It can be observed that the application of pre-stretch increases the maximal *actuation stretch* $\lambda_i^{max}/\lambda_i^0$, a characteristic which is eagerly pursued in sensors and actuators (Zhao & Suo, 2007). Here $\lambda_i^0 = (\lambda_z)^{-1/2}$ is the initial inner circumferential stretch induced by axial mechanical pre-stretch. Fig. 11(b) shows the effect of torsion $\bar{\gamma}$ on the deformation of the tube. We see that torsion can enhance the electro-elastic behavior of the solid by increasing the maximal allowable voltage.

6.2. Instability analysis

Fig. 12 presents the buckling behavior of a Mooney-Rivlin DE tube with $\bar{c}_1 = 0.9$, $\bar{R}_o = 1.4$ and subject to the axial constraint $\lambda_z = 1$ (no change in length) and $\bar{\gamma} = 0$ (no torsion). With the application of a radial voltage, the tube is expected to expand and elongate. Because of the axial constraint, compressive stresses may develop in the tube, which may lose its stability once the voltage exceeds a critical threshold. For a slender tube (small $\bar{k}$), the Euler buckling mode ($n = 1$) occurs first. In particular, an extremely thin tube with $\bar{k} \to 0$ is not able to sustain even a small compression, and the solid buckles

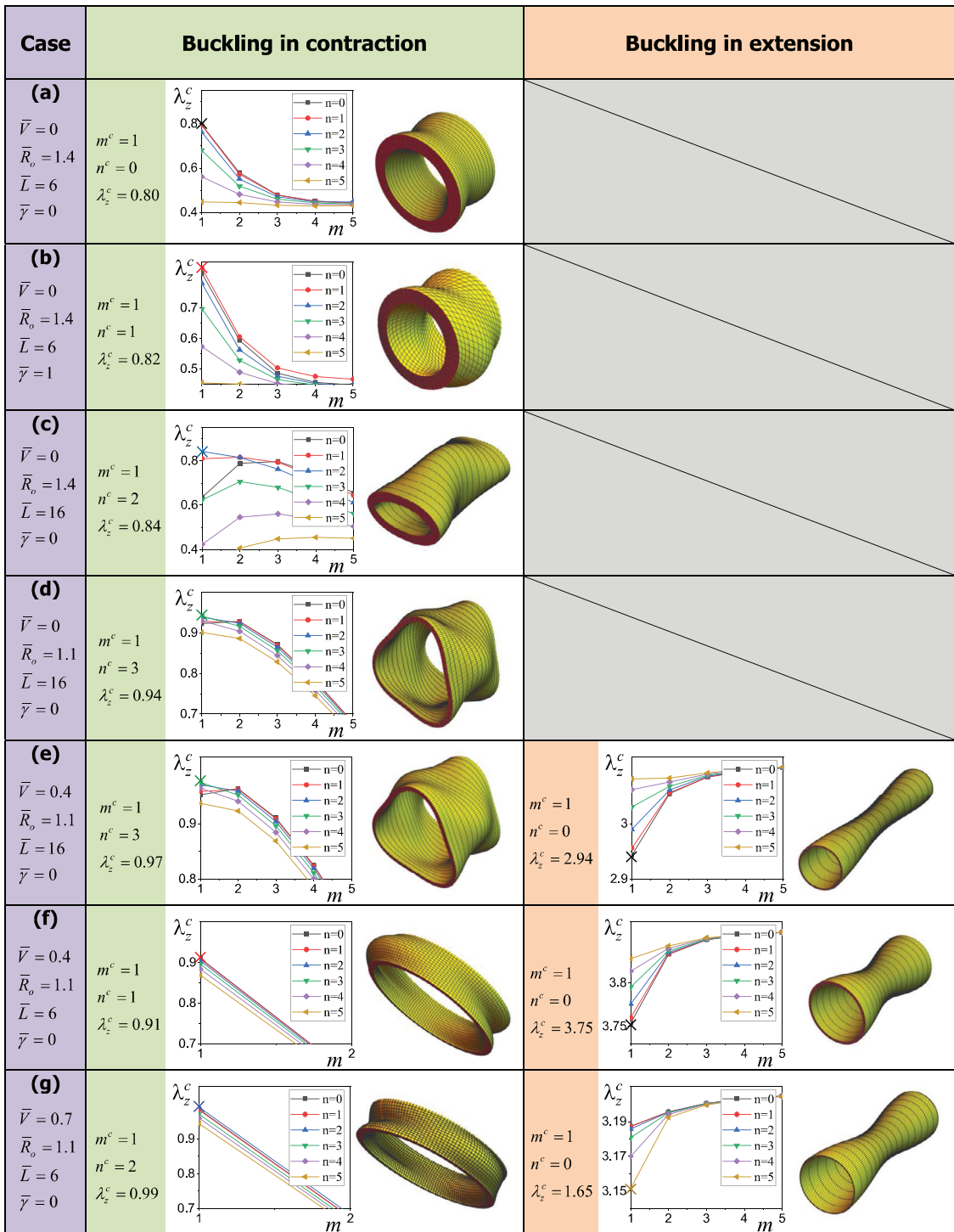**Fig. 10.** Effects of the voltage $\overline{V}$, radius ratio $\overline{R}_o$, torsion $\overline{\gamma}$ and length aspect ratio $\overline{L}$ on the buckling behavior of a DE tube. The critical points for buckling instability are marked by crosses.
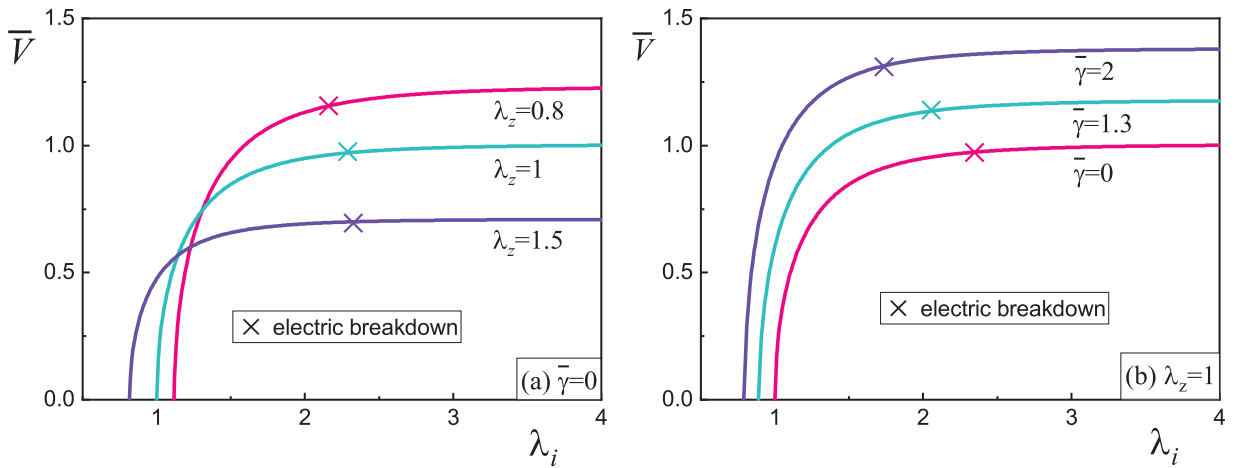
Fig. 11. Effects of (a) torsion $\overline{\gamma}$ and (b) axial pre-stretch λ_z on the $\overline{V} - \lambda_i$ response of a Mooney-Rivlin DE tube with $\overline{c}_1 = 0.9$ and $\overline{R}_o = 1.4$. The critical points for electric breakdown are marked by crosses.
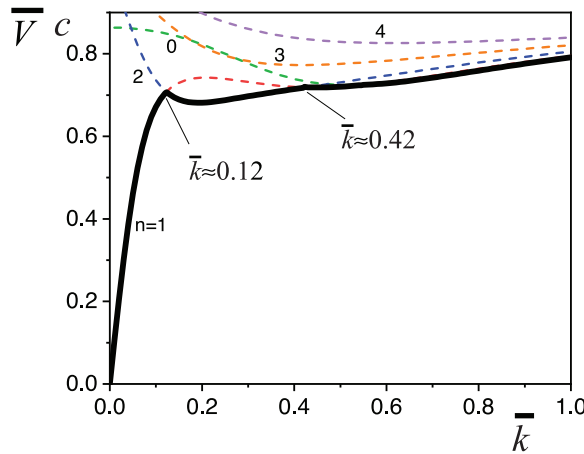

Fig. 12. Plots of the critical voltage $\overline{V}^c$ versus the dimensionless axial wave number $\overline{k}$ for buckling of a Mooney-Rivlin DE tube with $\overline{c}_1 = 0.9$, $\overline{R}_o = 1.4$ and subject to $\lambda_z = 1$ and $\overline{\gamma} = 0$ for a range of mode numbers $n = 0, 1, \ldots, 4$.

as soon as a small voltage is applied. Other buckling modes are induced as $\overline{k}$ increases: $n = 1$ for $0 \leq \overline{k} \leq 0.12$, $n = 2$ for $0.12 \leq \overline{k} \leq 0.42$, $n = 0$ for $\overline{k} \geq 0.42$.

In Fig. 13 we show the influence of axial pre-stretch λ_z on the transition and competitive mechanism between buckling and electric breakdown in the tube (note for Problem II, there is no pull-in instability).

We see from Case (a) in the figure that for a slender tube with $\overline{k} \leq 0.1$, the pre-compression $\lambda_z = 0.9$ is sufficient to make the tube buckle. By contrast, a thicker tube with $\overline{k} > 0.1$ can sustain the pre-compression: it eventually loses its stability with the application of an additional radial voltage $\overline{V}$. Then buckling always occurs first, and the electric breakdown criterion is not reached. It follows that in principle, we can design and fabricate voltage-induced smart surfaces and patterns in compressed solids ($\lambda_z < 1$) without encountering material failure.

In Case (b), where $\lambda_z = 2.5$, and Case (c), where $\lambda_z = 3.5$, we see that the application of a pre-stretch ($\lambda_z > 1$) shifts the threshold for buckling upward and the threshold for electric breakdown downward, respectively. When the pre-stretch is $\lambda_z = 2.5$, buckling occurs first in slender tubes, while electric breakdown is the dominant failure for thick tubes. The transition from one instability to the other occurs at $\overline{k} \approx 0.1$. When the pre-stretch is large (e.g., $\lambda_z = 3.5$), the solid always fails by electric breakdown first, as the voltage exceeds a threshold value. In that case, it is not possible to design and fabricate stable patterns for the tube. Notice that a tube subject to large pre-stretch always buckles in the mode $m^c = 1$, $n^c = 0$.

Fig. 14 presents the effect of torsion on the transition and competitive mechanism between buckling and electric breakdown of the voltage-actuated tube. We see that for an axially constrained ($\lambda_z = 1$ here) slender tube, the applied torsion will lead to buckling due to the Poynting effect. A thicker tube with larger $\overline{k}$ can sustain the torsion and an additional radial
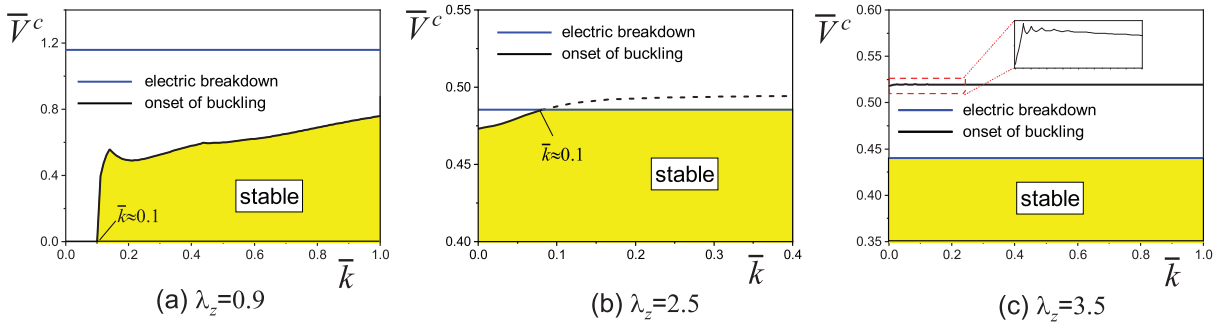
Fig. 13. Transition and competition between buckling and electric breakdown of Mooney-Rivlin DE tubes with $\bar{c}_1 = 0.9$, $\bar{\gamma} = 0$ and $\bar{R}_o = 1.4$ subject to varying axial constraints $\lambda_z = 0.9, 2.5, 3.5$. In this problem, the pull-in instability of the solid is suppressed. The black solid line corresponds to the meaningful dispersion curve for buckling instability of the elastomer, and the blue solid line represents the onset of electric breakdown of the solid $\bar{E}_{ri} = \bar{E}^B = 2$. (For interpretation of the references to color in this figure legend, the reader is referred to the web version of this article.)
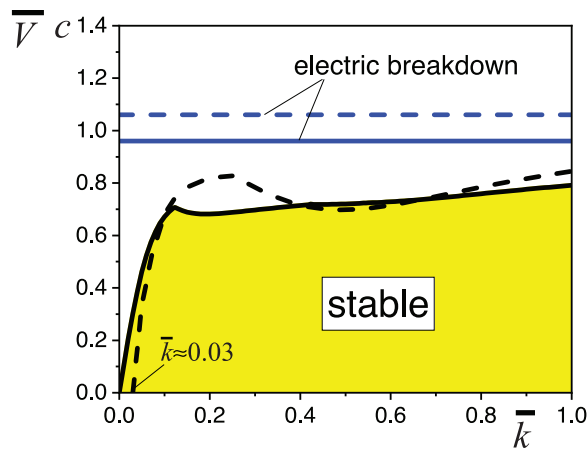

Fig. 14. Effect of torsion on the transition and competition between buckling and electric breakdown of Mooney-Rivlin DE tubes with $\bar{c}_1 = 0.9$, $\lambda_z = 1$ and $\bar{R}_o = 1.4$ (problem II). The black and blue solid lines correspond to the buckling and electric breakdown curves of the elastomer with no torsion ($\bar{\gamma} = 0$), respectively, and the black and blue dashed lines represent the buckling and electric breakdown curves of the elastomer subject to a torsion $\bar{\gamma} = 2$, respectively. (For interpretation of the references to color in this figure legend, the reader is referred to the web version of this article.)

voltage is required to buckle it. Note that the applied torsion can enhance the DE tube by increasing the critical electric breakdown voltage.

7. Conclusion

In conclusion, we have investigated the influences of the applied voltage, mechanical loading, structural geometry and actuation method on the finite response and incremental buckling behavior of a DE tube. Additionally, we also considered the pull-in (snap-through) instability and electric breakdown of the elastomer, and compared the transition and competitive mechanisms between these failures. In particular, two alternative problems were considered: Force tuning (Problem I) and voltage tuning (Problem II).

In the first problem (I), we found that the thinning of the tube will induce a competitive effect between the voltage and the mechanical force. The applied voltage increases the critical value of the voltage for buckling of the solid and creates the possibility of extensional buckling, which is absent in a purely elastic elastomer. Various buckling modes (m, n) can be selected for contractile buckling by tuning the length and thickness of the tube. While for extensional buckling, the tube always buckles in a trumpet-shape ($m = 1, n = 0$).

In the second problem (II), the $\bar{V} - \lambda_i$ curve is monotonic, and the snap-through instability of the solid will be suppressed. For the purely elastic case $\bar{V} = 0$, a slender tube with small $\bar{k}$ cannot sustain even a small axial compression ($\lambda_z < 1$) and will lose its stability immediately. The applied axial pre-stretch will increase the voltage threshold for buckling and decrease that for electric breakdown. As a result, electric breakdown will be the dominant failure mode in the solid when the pre-stretch is sufficiently large.

Due to the Poynting effect, the DE tube elongates with torsion $\bar{\gamma}$. For both cases, the critical electric breakdown voltage of the tube can be increased by introducing torsion. We proposed the approaches for designing stable structural patterns on

demand, without encountering material failure: Increasing the radial voltage $\overline{V}$ for problem I or decreasing the axial force $\overline{F}$ for problem II.

Declaration of Competing Interest

Authors declare that they have no conflict of interest.

Acknowledgments

Appendix A. Non-zero electro-elastic moduli

For the considered problem, the non-zero components of the instantaneous electro-elastic moduli for ideal dielectrics (39) read

$$
\begin{aligned}
\mathcal{A}_{1111} = {}& 2\lambda^{-4}\lambda_z^{-4}\big\{\lambda^2\big[4\Omega_{12}+\lambda_z^4(\Omega_2+\Omega_2\gamma^2 r^2)+\lambda_z^2(\Omega_1+4\Omega_{22}+4\Omega_{22}\gamma^2 r^2)\big] \\
&+2\big[\Omega_{11}+\lambda_z^2(1+\gamma^2 r^2)(2\Omega_{12}+\lambda_z^2\Omega_{22}+\lambda_z^2\gamma^2 r^2\Omega_{22})\big]+\lambda^4(\lambda_z^2\Omega_2+2\Omega_{22}+\lambda_z^4 D_r^4\Omega_5)\big\},
\end{aligned}
$$

$$
\begin{aligned}
\mathcal{A}_{1122} = {}& 4\lambda^{-4}\lambda_z^{-4}\big\{\lambda^6\lambda_z^2(\Omega_{12}+\lambda_z^2\Omega_{22})+\lambda_z^2\gamma^2 r^2\big[\Omega_{12}+\lambda_z^2(1+\gamma^2 r^2)\Omega_{22}\big] \\
&+\lambda^2\big[\Omega_{12}+r^4\gamma^4\lambda_z^6\Omega_{12}+\lambda_z^2\Omega_{22}+r^2\gamma^2\lambda_z^2\big(\lambda_z^4\Omega_{12}+\lambda_z^2\Omega_{11}+\lambda_z^2\Omega_2+2\Omega_{22}\big)\big] \\
&+\lambda^4\big[2\lambda_z^4(\Omega_{12}+r^2\gamma^2\Omega_{12})+\lambda_z^2(\Omega_{11}+\Omega_2)+\Omega_{22}+\lambda_z^6(\Omega_{22}+r^2\gamma^2\Omega_{22})\big]\big\},
\end{aligned}
$$

$$
\begin{aligned}
\mathcal{A}_{1123} =\mathcal{A}_{1132} = {}& 4\lambda^{-4}\lambda_z^{-2}r\gamma\big\{\Omega_{12}+\lambda^4\lambda_z^2\Omega_{12}+(1+r^2\gamma^2)\lambda_z^2\Omega_{22} \\
&+\lambda^2\big[\lambda_z^4(\Omega_{12}+r^2\gamma^2\Omega_{12})+\lambda_z^2(\Omega_{11}+\Omega_2)+\Omega_{22}\big]\big\},
\end{aligned}
$$

$$
\begin{aligned}
\mathcal{A}_{1133} = {}& 4\lambda^{-4}\lambda_z^{-2}\big\{\Omega_{12}+(1+r^2\gamma^2)\lambda_z^2\Omega_{22}+\lambda^6\lambda_z^2\Omega_{22} \\
&+\lambda^2\big[\lambda_z^4(\Omega_{12}+r^2\gamma^2\Omega_{12})+\lambda_z^2(\Omega_{11}+\Omega_2)+\Omega_{22}\big]+\lambda^4\big[2\lambda_z^2\Omega_{12}+\lambda_z^4(\Omega_{22}+r^2\gamma^2\Omega_{22})\big]\big\},
\end{aligned}
$$

$$
\mathcal{A}_{1212} = 2\lambda_z^{-2}\lambda^{-2}(\Omega_1+\lambda_z^2\Omega_2+D_r^2\lambda_z^2\lambda^2\Omega_5),
$$

$$
\mathcal{A}_{1213} = \mathcal{A}_{1231} = \mathcal{A}_{1321} = -2\lambda^{-2}r\gamma\Omega_2, \qquad \mathcal{A}_{1221} = -2\lambda^{-2}r^2\gamma^2\Omega_2-2\lambda_z^{-2}\Omega_2,
$$

$$
\mathcal{A}_{1313} = 2\lambda^{-2}\lambda_z^{-2}\big[\Omega_1+r^2\gamma^2\lambda_z^2\Omega_2+\lambda^2(\Omega_2+D_r^2\lambda_z^2\Omega_5)\big], \qquad \mathcal{A}_{1331} = -2\lambda^{-2}\Omega_2,
$$

$$
\mathcal{A}_{2121} = 2\big[r^2\gamma^2\lambda_z^2\Omega_1+\lambda^2(\Omega_1+\lambda_z^2\Omega_2)\big], \qquad \mathcal{A}_{2131} = 2r\gamma\lambda_z^2\Omega_1,
$$

$$
\begin{aligned}
\mathcal{A}_{2222} = {}& 2\lambda^{-4}\lambda_z^4\big\{2r^4\gamma^4\lambda_z^4\Omega_{22}+r^2\gamma^2\lambda^2\lambda_z^2(4r^2\gamma^2\lambda_z^4\Omega_{12}+\lambda_z^2\Omega_2+4\Omega_{22}) \\
&+2\lambda^8\lambda_z^4(\Omega_{11}+2\lambda_z^2\Omega_{12}+\lambda_z^4\Omega_{22}) \\
&+\lambda^6\big[4\lambda_z^2\Omega_{12}+4r^2\gamma^2\lambda_z^8\Omega_{12}+\lambda_z^6(4r^2\gamma^2\Omega_{11}+\Omega_2)+\lambda_z^4(\Omega_1+4\Omega_{22})\big] \\
&+\lambda^4\big[2r^4\gamma^4\lambda_z^8\Omega_{11}+\lambda_z^2\Omega_2+2\Omega_{22}+8r^2\gamma^2\lambda_z^4\Omega_{12}+r^2\gamma^2\lambda_z^6(\Omega_1+4\Omega_{22})\big]\big\},
\end{aligned}
$$

$$
\begin{aligned}
\mathcal{A}_{2223} = {}& 4r\gamma\lambda^{-4}\lambda^{-2}\big[\lambda^6\lambda_z^4(\Omega_{11}+\lambda_z^2\Omega_{12})+r^2\gamma^2\lambda_z^2\Omega_{22}+\lambda^2(2r^2\gamma^2\lambda_z^4\Omega_{12}+\Omega_{22}) \\
&+\lambda^4(r^2\gamma^2\lambda_z^6\Omega_{11}+2\lambda_z^2\Omega_{12}+\lambda_z^4\Omega_{22})\big]
\end{aligned}
$$

$$
\begin{aligned}
\mathcal{A}_{2232} = {}& 2r\gamma\lambda^{-4}\lambda_z^{-2}\big\{2\lambda^6\lambda_z^4(\Omega_{11}+\lambda_z^2\Omega_{12})+2r^2\gamma^2\lambda_z^2\Omega_{22}+\lambda^2(4r^2\gamma^2\lambda_z^4\Omega_{12}+\lambda_z^2\Omega_2+2\Omega_{22}) \\
&+\lambda^4\big[2r^2\gamma^2\lambda_z^6\Omega_{11}+4\lambda_z^2\Omega_{12}+\lambda_z^4(\Omega_1+2\Omega_{22})\big]\big\},
\end{aligned}
$$

$$
\begin{aligned}
\mathcal{A}_{2233} = {}& 4\lambda^{-4}\lambda_z^{-2}\big\{r^2\gamma^2\lambda_z^2\Omega_{22}+\lambda^2(2r^2\gamma^2\lambda_z^4\Omega_{12}+\Omega_{22}) \\
&+\lambda^6\lambda_z^2\big[\lambda_z^4(\Omega_{12}+r^2\gamma^2\Omega_{12})+\lambda_z^2(\Omega_{11}+\Omega_2)+\Omega_{22}\big] \\
&+\lambda^8\lambda_z^4(\Omega_{12}+\lambda_z^2\Omega_{22})+\lambda^4\big[2\lambda_z^2\Omega_{12}+\lambda_z^4\Omega_{22}+r^2\gamma^2\lambda_z^4(\lambda_z^2\Omega_{11}+\Omega_{22})\big]\big\},
\end{aligned}
$$

$$
\begin{aligned}
\mathcal{A}_{2323} = {}& 2\lambda^{-4}\lambda_z^{-2}\big\{\lambda^6\lambda_z^2\Omega_1+\lambda^4\big[r^2\gamma^2\lambda_z^4(\Omega_1+2\lambda_z^2\Omega_{11})+\Omega_2\big] \\
&r^2\gamma^2\lambda^2\lambda_z^2(4\lambda_z^2\Omega_{12}+\Omega_2)+2r^2\gamma^2\lambda_z^2\Omega_{22}\big\},
\end{aligned}
$$

$$
\mathcal{A}_{2332} = \lambda^{-4}\big[-2\lambda^6\lambda_z^2\Omega_2+4r^2\gamma^2(\lambda^4\lambda_z^4\Omega_{11}+2\lambda^2\lambda_z^2\Omega_{12}+\Omega_{22})\big],
$$

$$\mathcal{A}_{2333} = 2r\gamma\lambda^{-4}\{2\lambda^6\lambda_z^4\Omega_{12} + \lambda^2(4\lambda_z^2\Omega_{12} + \Omega_2) + 2\Omega_{22} + \lambda^4\lambda_z^2[\Omega_1 + 2(\lambda_z^2\Omega_{11} + \Omega_{22})]\},$$

$$\mathcal{A}_{3131} = 2\lambda_z^2(\Omega_1 + \lambda^2\Omega_2),$$

$$\mathcal{A}_{3232} = 2\lambda^{-4}[\lambda^4\lambda_z^2(\Omega_1 + 2r^2\gamma^2\lambda_z^2\Omega_{11}) + \lambda^2(4r^2\gamma^2\lambda_z^2\Omega_{12} + \Omega_2) + 2r^2\gamma^2\Omega_{22}],$$

$$\mathcal{A}_{3233} = 4\lambda^{-4}r\gamma[2\lambda^2\lambda_z^2\Omega_{12} + \lambda^6\lambda_z^4\Omega_{12} + \Omega_{22} + \lambda^4\lambda_z^2(\lambda_z^2\Omega_{11} + \Omega_{22})],$$

$$\mathcal{A}_{3333} = 2\lambda^{-4}[\lambda^2(4\lambda_z^2\Omega_{12} + \Omega_2) + \lambda^6\lambda_z^2(4\lambda_z^2\Omega_{12} + \Omega_2) + 2\Omega_{22}$$
$$+ 2\lambda^8\lambda_z^4\Omega_{22} + \lambda^4\lambda_z^2(\Omega_1 + 2\lambda_z^2\Omega_{11} + 4\Omega_{22})]. \tag{A.1}$$

$$\Gamma_{111}/2 = \Gamma_{122} = \Gamma_{133} = \Gamma_{212} = \Gamma_{313} = 2D_r\Omega_5. \tag{A.2}$$

$$K_{11} = K_{22} = K_{33} = 2\Omega_5. \tag{A.3}$$

Appendix B. Derivation of the Stroh formulation

The components of the incremental stress and electric field (22) for the ideal dielectric material can be expanded as

$$\dot{T}_{rr} = (\mathcal{A}_{1111} + p)\frac{\partial u_r}{\partial r} + \mathcal{A}_{1122}\frac{1}{r}\left(\frac{\partial u_\theta}{\partial\theta} + u_r\right) + \mathcal{A}_{1123}\left(\frac{1}{r}\frac{\partial u_z}{\partial\theta} + \frac{\partial u_\theta}{\partial z}\right)$$
$$+ \mathcal{A}_{1133}\frac{\partial u_z}{\partial z} + \Gamma_{111}\dot{D}_r - \dot{p},$$

$$\dot{T}_{\theta\theta} = \mathcal{A}_{1122}\frac{\partial u_r}{\partial r} + (\mathcal{A}_{2222} + p)\frac{1}{r}\left(\frac{\partial u_\theta}{\partial\theta} + u_r\right) + \mathcal{A}_{2232}\frac{\partial u_\theta}{\partial z} + \mathcal{A}_{2223}\frac{1}{r}\frac{\partial u_z}{\partial\theta}$$
$$+ \mathcal{A}_{2233}\frac{\partial u_z}{\partial z} + \Gamma_{221}\dot{D}_r - \dot{p},$$

$$\dot{T}_{zz} = \mathcal{A}_{1133}\frac{\partial u_r}{\partial r} + \mathcal{A}_{2233}\frac{1}{r}\left(\frac{\partial u_\theta}{\partial\theta} + u_r\right) + \mathcal{A}_{2333}\frac{1}{r}\frac{\partial u_z}{\partial\theta} + \mathcal{A}_{3233}\frac{\partial u_\theta}{\partial z}$$
$$+ (\mathcal{A}_{3333} + p)\frac{\partial u_z}{\partial z} + \Gamma_{0331}\dot{D}_r - \dot{p},$$

$$\dot{T}_{r\theta} = \mathcal{A}_{1212}\frac{\partial u_\theta}{\partial r} + (\mathcal{A}_{1221} + p)\frac{1}{r}\left(\frac{\partial u_r}{\partial\theta} - u_\theta\right) + \mathcal{A}_{1213}\left(\frac{\partial u_z}{\partial r} + \frac{\partial u_r}{\partial z}\right) + \Gamma_{122}\dot{D}_\theta,$$

$$\dot{T}_{rz} = \mathcal{A}_{1313}\frac{\partial u_z}{\partial r} + (\mathcal{A}_{1331} + p)\frac{\partial u_r}{\partial z} + \mathcal{A}_{1312}\left[\frac{\partial u_\theta}{\partial r} + \frac{1}{r}\left(\frac{\partial u_r}{\partial\theta} - u_\theta\right)\right] + \Gamma_{133}\dot{D}_z,$$

$$\dot{T}_{\theta r} = \mathcal{A}_{2121}\frac{1}{r}\left(\frac{\partial u_r}{\partial\theta} - u_\theta\right) + (\mathcal{A}_{1221} + p)\frac{\partial u_\theta}{\partial r} + \mathcal{A}_{2113}\frac{\partial u_z}{\partial r} + \mathcal{A}_{2131}\frac{\partial u_r}{\partial z} + \Gamma_{122}\dot{D}_\theta,$$

$$\dot{T}_{\theta z} = \mathcal{A}_{2323}\frac{1}{r}\frac{\partial u_z}{\partial\theta} + (\mathcal{A}_{2332} + p)\frac{\partial u_\theta}{\partial z} + \mathcal{A}_{2223}\frac{1}{r}\left(\frac{\partial u_\theta}{\partial\theta} + u_r\right) + \mathcal{A}_{2311}\frac{\partial u_r}{\partial r} + \mathcal{A}_{2333}\frac{\partial u_z}{\partial z},$$

$$\dot{T}_{zr} = \mathcal{A}_{3131}\frac{\partial u_r}{\partial z} + (\mathcal{A}_{1331} + p)\frac{\partial u_z}{\partial r} + \mathcal{A}_{3112}\frac{\partial u_\theta}{\partial r} + \mathcal{A}_{3121}\frac{1}{r}\left(\frac{\partial u_r}{\partial\theta} - u_\theta\right) + \Gamma_{133}\dot{D}_z,$$

$$\dot{T}_{z\theta} = \mathcal{A}_{3232}\frac{\partial u_\theta}{\partial z} + (\mathcal{A}_{2332} + p)\frac{1}{r}\frac{\partial u_z}{\partial\theta} + \mathcal{A}_{3211}\frac{\partial u_r}{\partial r} + \mathcal{A}_{3222}\frac{1}{r}\left(\frac{\partial u_\theta}{\partial\theta} + u_r\right) + \mathcal{A}_{3233}\frac{\partial u_z}{\partial z},$$

$$\dot{E}_r = -\frac{\partial\dot{\phi}}{\partial r} = \Gamma_{111}\frac{\partial u_r}{\partial r} + \Gamma_{221}\frac{1}{r}\left(\frac{\partial u_\theta}{\partial\theta} + u_r\right) + \Gamma_{331}\frac{\partial u_z}{\partial z} + K_{11}\dot{D}_r,$$

$$\dot{E}_\theta = -\frac{1}{r}\frac{\partial\dot{\phi}}{\partial\theta} = \Gamma_{122}\left[\frac{1}{r}\left(\frac{\partial u_r}{\partial\theta} - u_\theta\right) + \frac{\partial u_\theta}{\partial r}\right] + K_{22}\dot{D}_\theta,$$

$$\dot{E}_z = -\frac{\partial \dot{\phi}}{\partial z} = \Gamma_{133}\left(\frac{\partial u_r}{\partial z} + \frac{\partial u_z}{\partial_r}\right) + K_{33}\dot{D}_z. \tag{B.1}$$

The components of the incremental equilibrium Eq. (20)$_1$ and the incremental Maxwell Eq. (20)$_2$ are

$$\frac{\partial \dot{T}_{0rr}}{\partial r} + \frac{1}{r}\frac{\partial \dot{T}_{0\theta r}}{\partial \theta} + \frac{\dot{T}_{0rr} - \dot{T}_{0\theta\theta}}{r} + \frac{\partial \dot{T}_{0zr}}{\partial z} = 0,$$

$$\frac{\partial \dot{T}_{0r\theta}}{\partial r} + \frac{1}{r}\frac{\partial \dot{T}_{0\theta\theta}}{\partial \theta} + \frac{\dot{T}_{0\theta r} + \dot{T}_{0r\theta}}{r} + \frac{\partial \dot{T}_{0z\theta}}{\partial z} = 0,$$

$$\frac{\partial \dot{T}_{0rz}}{\partial r} + \frac{1}{r}\frac{\partial \dot{T}_{0\theta z}}{\partial \theta} + \frac{\partial \dot{T}_{0zz}}{\partial z} + \frac{\dot{T}_{0rz}}{r} = 0, \tag{B.2}$$

and

$$\frac{\partial \dot{D}_{l0r}}{\partial r} + \frac{1}{r}\left(\frac{\partial \dot{D}_{l0\theta}}{\partial \theta} + \dot{D}_{l0r}\right) + \frac{\partial \dot{D}_{l0z}}{\partial z} = 0, \tag{B.3}$$

respectively.

The incompressibility condition Eq. (21) for the incremental motion reads

$$\frac{\partial u_r}{\partial r} + \frac{1}{r}\left(\frac{\partial u_\theta}{\partial \theta} + u_r\right) + \frac{\partial u_z}{\partial z} = 0. \tag{B.4}$$

First, rewriting Eq. (B.4) using solutions (24) gives

$$U_r' = \frac{i}{r}(iU_r - nU_\theta - krU_z). \tag{B.5}$$

Next, from Eqs. (B.1)$_{4,5,11,12}$ and (24) we obtain

$$U_\theta' = \frac{i}{r}[a_1 U_r + ia_2 U_\theta + a_3(ir\Sigma_{r\theta}) + a_4(ir\Sigma_{rz}) + a_5\Phi],$$

$$U_z' = \frac{i}{r}[b_1 U_r + ib_2 U_\theta + b_3(ir\Sigma_{r\theta}) + b_4(ir\Sigma_{rz}) + b_5\Phi], \tag{B.6}$$

where

$$a_1 = -n + \frac{(\mathcal{A}_{1213}kr - n\gamma_{13})\tau_{rr}}{\mathcal{A}_{1213}^2 - \gamma_{12}\gamma_{13}}, \quad b_1 = -kr + \frac{(\mathcal{A}_{1213}n - kr\gamma_{12})\tau_{rr}}{\mathcal{A}_{1213}^2 - \gamma_{12}\gamma_{13}},$$

$$a_2 = -1 - \frac{\gamma_{13}\tau_{rr}}{\mathcal{A}_{1213}^2 - \gamma_{12}\gamma_{13}}, \quad b_2 = \frac{\mathcal{A}_{1213}\tau_{rr}}{\mathcal{A}_{1213}^2 - \gamma_{12}\gamma_{13}},$$

$$a_3 = \frac{\gamma_{13}}{\mathcal{A}_{1213}^2 - \gamma_{12}\gamma_{13}}, \quad b_4 = \frac{\gamma_{12}}{\mathcal{A}_{1213}^2 - \gamma_{12}\gamma_{13}},$$

$$a_4 = b_3 = \frac{\mathcal{A}_{1213}}{-\mathcal{A}_{1213}^2 + \gamma_{12}\gamma_{13}}, \quad b_5 = \frac{\mathcal{A}_{1213}nK_{33}\Gamma_{122} - K_{22}kr\Gamma_{133}\gamma_{12}}{\mathcal{A}_{1213}^2 K_{22}K_{33} - K_{22}K_{33}\gamma_{12}\gamma_{13}},$$

$$a_5 = \frac{\mathcal{A}_{1213}krK_{22}\Gamma_{133} - K_{33}n\Gamma_{122}\gamma_{13}}{\mathcal{A}_{1213}^2 K_{22}K_{33} - K_{22}K_{33}\gamma_{12}\gamma_{13}},$$

$$\gamma_{12} = \mathcal{A}_{1212} - \frac{\Gamma_{122}^2}{K_{22}}, \quad \gamma_{13} = \mathcal{A}_{1313} - \frac{\Gamma_{133}^2}{K_{33}}. \tag{B.7}$$

Substitution of Eqs. (B.1)$_{11,12}$ and (24) into Eq. (B.2)$_1$ results in

$$(ir\Delta_r)' = \frac{i}{r}\left\{-\left[\frac{n\Gamma_{122}}{K_{22}}(n + a_1) + \frac{kr\Gamma_{133}}{K_{33}}(kr + b_1)\right]U_r - i\left[\frac{n\Gamma_{122}}{K_{22}}(1 + a_2) + \frac{kr\Gamma_{133}b_2}{K_{33}}\right]U_\theta\right.$$

$$-\left(\frac{\Gamma_{122}n}{K_{22}}a_3 + \frac{\Gamma_{133}kr}{K_{33}}b_3\right)(ir\Sigma_{r\theta}) - \left(\frac{\Gamma_{122}n}{K_{22}}a_4 + \frac{\Gamma_{133}kr}{K_{33}}b_4\right)(ir\Sigma_{rz})$$

$$\left. -\left(\frac{n^2}{K_{22}} + \frac{k^2r^2}{K_{33}} + \frac{\Gamma_{122}n}{K_{22}}a_5 + \frac{\Gamma_{133}kr}{K_{33}}b_5\right)\Phi\right\}. \tag{B.8}$$

We then substitute Eqs. (B.1)$_{1,2,6,8,11,12}$ and into Eq. (B.2)$_1$ and use the solution (24) to get

$$
\begin{aligned}
(\mathrm{i}r\Sigma_{rr})' = \frac{\mathrm{i}}{r}\big[&\kappa_{11}U_r + \mathrm{i}\kappa_{12}U_\theta + \mathrm{i}\kappa_{13}U_z + \mathrm{i}(\Gamma_{111} - \Gamma_{221})(\mathrm{i}r\Delta_r) - \mathrm{i}(\mathrm{i}r\Sigma_{rr}) \\
&+ (xa_3 + yb_3)(\mathrm{i}r\Sigma_{r\theta}) + (xa_4 + yb_4)(\mathrm{i}r\Sigma_{rz}) \\
&+ \left(xa_5 + yb_5 - \frac{\Gamma_{122}n^2}{K_{22}} - \frac{\Gamma_{133}k^2 r^2}{K_{33}} \right)\Phi \big],
\end{aligned}
\tag{B.9}
$$

where

$$
\begin{aligned}
x &= (\gamma_{12} - \tau_{rr})n + kr\mathcal{A}_{1231}, \qquad y = (\gamma_{13} - \tau_{rr})kr + n\mathcal{A}_{1321}, \\
\kappa_{11} &= 2(\gamma_{12} - \tau_{rr} + \beta_{12}) + \gamma_{21}n^2 + \gamma_{31}k^2 r^2 + 2\mathcal{A}_{3121}nkr + xa_1 + yb_1, \\
\kappa_{12} &= n[2\beta_{12} + 2(\gamma_{12} - \tau_{rr}) + \gamma_{21}] - kr(\mathcal{A}_{1123} - \mathcal{A}_{2232} - \mathcal{A}_{2131}) + xa_2 + yb_2, \\
\kappa_{13} &= kr(\mathcal{A}_{01111} + \mathcal{A}_{02233} - \mathcal{A}_{01122} - \mathcal{A}_{01133} + p) - n(\mathcal{A}_{1123} - \mathcal{A}_{2223}), \\
\gamma_{21} &= \mathcal{A}_{2121} - \frac{\Gamma_{122}^2}{K_{22}}, \qquad \gamma_{31} = \mathcal{A}_{3131} - \frac{\Gamma_{133}^2}{K_{33}}, \\
\beta_{12} &= \frac{1}{2}\left(\mathcal{A}_{1111} + \mathcal{A}_{2222} - 2\mathcal{A}_{1122} - 2\mathcal{A}_{1221} + \frac{2\Gamma_{122}^2}{K_{22}} \right).
\end{aligned}
\tag{B.10}
$$

Similarly, the remaining equilibrium Eqs. (B.2)$_{2,3}$ can be rearranged to get

$$
\begin{aligned}
(\mathrm{i}r\Sigma_{r\theta})' = \frac{\mathrm{i}}{r}\big\{ &-\mathrm{i}\kappa_{12}U_r + \kappa_{22}U_\theta + \kappa_{23}U_z - n(\mathrm{i}r\Sigma_{rr}) - \mathrm{i}[(\gamma_{12} - \tau_{rr})a_3 + \mathcal{A}_{2113}b_3](\mathrm{i}r\Sigma_{r\theta}) \\
&-\mathrm{i}[(\gamma_{12} - \tau_{rr})a_4 + \mathcal{A}_{2113}b_4](\mathrm{i}r\Sigma_{rz}) - n(\Gamma_{221} - \Gamma_{111})(\mathrm{i}r\Delta_r) \\
&-\mathrm{i}\left[(\gamma_{12} - \tau_{rr})a_5 + \mathcal{A}_{1321}b_5 + \frac{\Gamma_{122}n}{K_{22}} \right]\Phi \big\}, \\
(\mathrm{i}r\Sigma_{rz})' = \frac{\mathrm{i}}{r}\big[&-\mathrm{i}\kappa_{13}U_r + \kappa_{23}U_\theta + \kappa_{33}U_z + kr(\Gamma_{111} - \Gamma_{331})(\mathrm{i}r\Delta_r) - kr(\mathrm{i}r\Sigma_{rr}) \big],
\end{aligned}
\tag{B.11}
$$

where

$$
\begin{aligned}
\kappa_{22} &= 2n^2(\gamma_{12} - \tau_{rr} + \beta_{12}) + \gamma_{21} + k^2 r^2 \mathcal{A}_{3232} \\
&\quad + 2nkr(\mathcal{A}_{2232} - \mathcal{A}_{1123}) + (\gamma_{12} - \tau_{rr})a_2 + \mathcal{A}_{1321}b_2, \\
\kappa_{23} &= nkr(\mathcal{A}_{1111} + \mathcal{A}_{2233} + \mathcal{A}_{2332} - \mathcal{A}_{1122} - \mathcal{A}_{1133} + 2p) - k^2 r^2(\mathcal{A}_{1132} - \mathcal{A}_{3233}) \\
&\quad - n^2(\mathcal{A}_{1123} - \mathcal{A}_{2223}), \\
\kappa_{33} &= k^2 r^2(\mathcal{A}_{1111} - 2\mathcal{A}_{1133} + \mathcal{A}_{3333} + 2p) + n^2 \mathcal{A}_{2323} - 2nkr(\mathcal{A}_{1123} - \mathcal{A}_{2223}).
\end{aligned}
\tag{B.12}
$$

Finally, from Eqs. (B.1)$_{10}$, (24) and (B.5), we have

$$
\Phi' = \frac{\mathrm{i}}{r}[-\mathrm{i}(\Gamma_{0111} - \Gamma_{0221})U_r + n(\Gamma_{0111} - \Gamma_{0221})U_\theta (\Gamma_{0111} - \Gamma_{0331})U_z + K_{011}(\mathrm{i}r\Delta_r)].
\tag{B.13}
$$

Now we can write Eqs. (B.5), (B.6), (B.8), (B.9), (B.11) and (B.13) in the form presented in Eq. (27), with the non-zero components of $\boldsymbol{G}^a$, $\boldsymbol{G}^b$ and $\boldsymbol{G}^c$ have the forms

$$
\begin{aligned}
&G_{11}^a = \mathrm{i}, \quad G_{12}^a = -n, \quad G_{13}^a = -kr, \quad G_{21}^a = a_1, \quad G_{22}^a = \mathrm{i}a_2, \\
&G_{31}^a = b_1, \quad G_{32}^a = \mathrm{i}b_2, \quad G_{41}^a = -\left[\frac{n\Gamma_{122}}{K_{22}}(n + a_1) + \frac{kr\Gamma_{133}}{K_{33}}(kr + b_1) \right], \\
&G_{42}^a = -\mathrm{i}\left[\frac{n\Gamma_{122}}{K_{22}}(1 + a_2) + \frac{kr\Gamma_{133}b_2}{K_{33}} \right], \\
&G_{22}^b = a_3, \quad G_{23}^b = G_{32}^b = a_4, \quad G_{24}^b = b_5, \quad G_{33}^b = b_4, \quad G_{34}^b = G_{43}^b = b_5, \\
&G_{44}^b = -\left(\frac{n^2}{K_{22}} + \frac{k^2 r^2}{K_{33}} + \frac{\Gamma_{122}n}{K_{22}}a_5 + \frac{\Gamma_{133}kr}{K_{33}}b_5 \right),
\end{aligned}
$$

$$G_{11}^c = \kappa_{11}, \quad G_{12}^c = -G_{21}^c = i\kappa_{12}, \quad G_{13}^c = -G_{31}^c = i\kappa_{13},$$

$$G_{14}^c = -G_{41}^c = i(\Gamma_{111} - \Gamma_{221}), \quad G_{22}^c = \kappa_{22}, \quad G_{23}^c = G_{32}^c = \kappa_{23},$$

$$G_{24}^c = G_{42}^c = n(\Gamma_{111} - \Gamma_{221}), \quad G_{34}^c = G_{43}^c = kr(\Gamma_{111} - \Gamma_{331}), \quad G_{44}^c = K_{11}. \tag{B.14}$$

References

Arora, S., Ghosh, T., & Muth, J. (2007). Dielectric elastomer based prototype fiber actuators. *Sensors and Actuators A: Physical, 136*(1), 321–328.

Batra, R. C., Mueller, I., & Strehlow, P. (2005). Treloar's biaxial tests and Kearsley's bifurcation in rubber sheets. *Mathematics and Mechanics of Solids, 10*(6), 705–713.

Bertoldi, K., & Gei, M. (2011). Instabilities in multilayered soft dielectrics. *Journal of the Mechanics and Physics of Solids, 59*(1), 18–42.

Biot, M. A. (1965). *Mechanics of incremental deformations*. New York: John Wiley.

Bortot, E., & Shmuel, G. (2018). Prismatic bifurcations of soft dielectric tubes. *International Journal of Engineering Science, 124*, 104–114.

Brochu, P., & Pei, Q. (2012). Dielectric elastomers for actuators and artificial muscles. In *Electroactivity in polymeric materials* (pp. 1–56)). Boston, MA: Springer.

Brown, N. M., & Lai, F. C. (2009). Electrohydrodynamic gas pump in a vertical tube. *Journal of Electrostatics, 67*(4), 709–714.

Cameron, C. G., Szabo, J. P., Johnstone, S., Massey, J., & Leidner, J. (2008). Linear actuation in coextruded dielectric elastomer tubes. *Sensors and Actuators A: Physical, 147*(1), 286–291.

Carpi, F., & De Rossi, D. (2004). Dielectric elastomer cylindrical actuators: electromechanical modelling and experimental evaluation. *Materials Science and Engineering: C, 24*(4), 555–562.

Che, S., Lu, T., & Wang, T. J. (2017). Electromechanical phase transition of a dielectric elastomer tube under internal pressure of constant mass. *Theoretical and Applied Mechanics Letters, 7*(3), 121–125.

Ciarletta, P., & Destrade, M. (2014). Torsion instability of soft solid cylinders. *The IMA Journal of Applied Mathematics, 79*(5), 804–819.

Destrade, M., Annaidh, A. N., & Coman, C. D. (2009). Bending instabilities of soft biological tissues. *International Journal of Solids and Structures, 46*(25–26), 4322–4330.

Dissado, L. A., & Fothergill, J. C. (1992). *Electrical degradation and breakdown in polymers*: 9. let.

Dorfmann, A., & Ogden, R. W. (2005). Nonlinear electroelasticity. *Acta Mechanica, 174*(3–4), 167–183.

Dorfmann, A., & Ogden, R. W. (2006). Nonlinear electroelastic deformations. *Journal of Elasticity, 82*(2), 99–127.

Dorfmann, L., & Ogden, R. W. (2016). *Nonlinear theory of electroelastic and magnetoelastic interactions*. New York: Springer.

Dorfmann, L., & Ogden, R. W. (2017). Nonlinear electroelasticity: Material properties, continuum theory and applications. *Proceedings of the Royal Society A: Mathematical, Physical and Engineering Sciences, 473*(2204), 20170311.

Duduta, M., Hajiesmaili, E., Zhao, H., Wood, R. J., & Clarke, D. R. (2019). Realizing the potential of dielectric elastomer artificial muscles. *Proceedings of the National Academy of Sciences, 116*(7), 2476–2481.

Fu, Y., Dorfmann, L., & Xie, Y. (2018a). Localized necking of a dielectric membrane. *Extreme Mechanics Letters, 21*, 44–48.

Fu, Y., Xie, Y., & Dorfmann, L. (2018b). A reduced model for electrodes-coated dielectric plates. *International Journal of Non-Linear Mechanics, 106*, 60–69.

Gei, M., Colonnelli, S., & Springhetti, R. (2014). The role of electrostriction on the stability of dielectric elastomer actuators. *International Journal of Solids and Structures, 51*(3–4), 848–860.

Getz, R., Kochmann, D. M., & Shmuel, G. (2017). Voltage-controlled complete stopbands in two-dimensional soft dielectrics. *International Journal of Solids and Structures, 113*, 24–36.

Goriely, A., Vandiver, R., & Destrade, M. (2008). Nonlinear euler buckling. *Proceedings of the Royal Society A: Mathematical, Physical and Engineering Sciences, 464*(2099), 3003–3019.

Goshkoderia, A., & Rudykh, S. (2017). Electromechanical macroscopic instabilities in soft dielectric elastomer composites with periodic microstructures. *European Journal of Mechanics-A/Solids, 65*, 243–256.

Huang, J., Li, T., Chiang Foo, C., Zhu, J., Clarke, D. R., & Suo, Z. (2012). Giant, voltage-actuated deformation of a dielectric elastomer under dead load. *Applied Physics Letters, 100*(4), 041911.

Lu, T., An, L., Li, J., Yuan, C., & Wang, T. J. (2015). Electro-mechanical coupling bifurcation and bulging propagation in a cylindrical dielectric elastomer tube. *Journal of the Mechanics and Physics of Solids, 85*, 160–175.

Melnikov, A., & Ogden, R. W. (2018). Bifurcation of finitely deformed thick-walled electroelastic cylindrical tubes subject to a radial electric field. *Zeitschrift fr angewandte Mathematik und Physik, 69*(3), 60.

Ogden, R. W. (1997). *Non-linear elastic deformations*. Courier Corporation.

O'Halloran, A., O'malley, F., & McHugh, P. (2008). A review on dielectric elastomer actuators, technology, applications, and challenges. *Journal of Applied Physics, 104*(7), 9.

Pang, W., Cheng, X., Zhao, H., Guo, X., Ji, Z., Li, G., … Zhang, Y. (2020). Electro-mechanically controlled assembly of reconfigurable 3D mesostructures and electronic devices based on dielectric elastomer platforms. *National Science Review, 7*(2), 342–354.

Pelrine, R., Kornbluh, R., Pei, Q., & Joseph, J. (2000). High-speed electrically actuated elastomers with strain greater than 100%. *Science, 287*(5454), 836–839.

Pelrine, R. E., Kornbluh, R. D., & Joseph, J. P. (1998). Electrostriction of polymer dielectrics with compliant electrodes as a means of actuation. *Sensors and Actuators A: Physical, 64*(1), 77–85.

Plante, J. S., & Dubowsky, S. (2006). Large-scale failure modes of dielectric elastomer actuators. *International Journal of Solids and Structures, 43*(25–26), 7727–7751.

Poya, R., Gil, A. J., Ortigosa, R., Sevilla, R., Bonet, J., & Wall, W. A. (2018). A curvilinear high order finite element framework for electromechanics: From linearised electro-elasticity to massively deformable dielectric elastomers. *Computer Methods in Applied Mechanics and Engineering, 329*, 75–117.

Rasmussen, L. (2012). *Electroactivity in polymeric materials*. Springer Science & Business Media.

Rivlin, R. S., & Saunders, D. W. (1951). Large elastic deformations of isotropic materials VII. Experiments on the deformation of rubber. *Philosophical Transactions of the Royal Society of London. Series A, Mathematical and Physical Sciences, 243*(865), 251–288.

Romeo, M. (2011). Micromorphic continuum model for electromagnetoelastic solids. *Zeitschrift für angewandte Mathematik und Physik, 62*(3), 513–527.

Shmuel, G., & deBotton, G. (2013). Axisymmetric wave propagation in finitely deformed dielectric elastomer tubes. *Proceedings of the Royal Society A: Mathematical, Physical and Engineering Sciences, 469*(2155), 20130071.

Singh, M. (1966). Controllable states in compressible elastic dielectrics. *Zeitschrift fr angewandte Mathematik und Physik ZAMP, 17*(3), 449–453.

Stark, K. H., & Garton, C. G. (1955). Electric strength of irradiated polythene. *Nature, 176*(4495), 1225–1226.

Stoyanov, H., Kofod, G., & Gerhard, R. (2008). A co-axial dielectric elastomer actuator. In *Advances in science and technology: 61* (pp. 81–84)). Trans Tech Publications.

Su, Y., Broderick, H. C., Chen, W., & Destrade, M. (2018). Wrinkles in soft dielectric plates. *Journal of the Mechanics and Physics of Solids, 119*, 298–318.

Su, Y., Wu, B., Chen, W., & Destrade, M. (2019). Finite bending and pattern evolution of the associated instability for a dielectric elastomer slab. *International Journal of Solids and Structures, 158*, 191–209.

Su, Y., Zhou, W., Chen, W., & Lü, C. (2016a). On buckling of a soft incompressible electroactive hollow cylinder. *International Journal of Solids and Structures, 97*, 400–416.

Su, Y. P., Wang, H. M., Zhang, C. L., & Chen, W. Q. (2016b). Propagation of non-axisymmetric waves in an infinite soft electroactive hollow cylinder under uniform biasing fields. *International Journal of Solids and Structures, 81*, 262–273.

Wang, F., Yuan, C., Lu, T., & Wang, T. J. (2017). Anomalous bulging behaviors of a dielectric elastomer balloon under internal pressure and electric actuation. *Journal of the Mechanics and Physics of Solids, 102*, 1–16.

Wang, Q., Gossweiler, G. R., Craig, S. L., & Zhao, X. (2014). Cephalopod-inspired design of electro-mechano-chemically responsive elastomers for on-demand fluorescent patterning. *Nature communications, 5*(1), 1–9.

Wang, Y., Li, Z., Qin, L., Caddy, G., Yap, C. H., & Zhu, J. (2018). Dielectric elastomer fluid pump of high pressure and large volume via synergistic snap-through. *Journal of Applied Mechanics, 85*(10), 121011 (7 pages).

Wu, B., Su, Y., Chen, W., & Zhang, C. (2017). On guided circumferential waves in soft electroactive tubes under radially inhomogeneous biasing fields. *Journal of the Mechanics and Physics of Solids, 99*, 116–145.

Yang, J., & Hu, Y. (2004). Mechanics of electroelastic bodies under biasing fields. *Applied Mechanics Review, 57*(3), 173–189.

Zhang, H., Wang, Y., Godaba, H., Khoo, B. C., Zhang, Z., & Zhu, J. (2017). Harnessing dielectric breakdown of dielectric elastomer to achieve large actuation. *Journal of applied mechanics, 84*(12).

Zhao, X., & Suo, Z. (2007). Method to analyze electromechanical stability of dielectric elastomers. *Applied Physics Letters, 91*(6), 061921.

Zhu, J., Stoyanov, H., Kofod, G., & Suo, Z. (2010). Large deformation and electromechanical instability of a dielectric elastomer tube actuator. *Journal of Applied Physics, 108*(7), 074113.

Zurlo, G., Destrade, M., DeTommasi, D., & Puglisi, G. (2017). Catastrophic thinning of dielectric elastomers. *Physical review letters, 118*(7), 078001.